CAIT-UTC-050

Effects of Temperature on Bridge Dynamic Properties

FINAL REPORT
December 2015

Submitted by:

Navid Zolghadri
PhD Student

Marvin W. Halling
Professor

Paul J. Barr
Professor

Nick Foust
Masters

Navid Zolghadri, Marvin W. Halling, Paul J. Barr, and Nick Foust
4110 Old Main Hill
Logan, UT 84332

In cooperation with
Rutgers, The State University of New Jersey
And
Utah Department of Transportation
And
U.S. Department of Transportation
Federal Highway Administration

Disclaimer Statement

The contents of this report reflect the views of the authors, who are responsible for the facts and the accuracy of the information presented herein. This document is disseminated under the sponsorship of the Department of Transportation, University Transportation Centers Program, in the interest of information exchange. The U.S. Government assumes no liability for the contents or use thereof.

The Center for Advanced Infrastructure and Transportation (CAIT) is a Tier I UTC Consortium led by Rutgers, The State University. Members of the consortium are the University of Delaware, Utah State University, Columbia University, New Jersey Institute of Technology, Princeton University, University of Texas at El Paso, University of Virginia and Virginia Polytechnic Institute. The Center is funded by the U.S. Department of Transportation.

TECHNICAL REPORT STANDARD TITLE PAGE

1. Report No.	2. Government Accession No.	3. Recipient's Catalog No.
CAIT-UTC-050		

4. Title and Subtitle	5. Report Date
Effects of Temperature on Bridge Dynamic Properties	December 2015
	6. Performing Organization Code CAIT/Utah State University
7. Author(s) Navid Zolghadri, Marvin W. Halling, Paul J. Barr, and Nick Foust	8. Performing Organization Report No. CAIT-UTC-050
9. Performing Organization Name and Address Utah State University 4110 Old Main Hill Logan, UT 84322	10. Work Unit No.
	11. Contract or Grant No. DTRT-G-UTC16
12. Sponsoring Agency Name and Address Center for Advanced Infrastructure and Transportation Rutgers, The State University of New Jersey 100 Brett Road Piscataway, NJ 08854	13. Type of Report and Period Covered Final Report 06/01/12 to 012/30/15
	14. Sponsoring Agency Code

15. Supplementary Notes

U.S. Department of Transportation/Research & Innovative Technology Administration
1200 New Jersey Avenue, SE
Washington, DC 20590-0001

16. Abstract

Structural health monitoring (SHM) using ambient vibration has become a valuable tool in evaluating and assessing the condition of civil structures. For bridge structures, a vibration-based SHM system uses the dynamic response of a bridge to measure modal parameters. A change in a structure's modal parameters can indicate a physical change in the system, such as damage or a boundary condition change. These same modal parameters are sensitive to environmental factors, mainly temperature. Statistical models have been utilized to filter out modal parameter changes influenced by temperature and those caused by physical changes. Statistical models also help describe the relationship between modal parameters and environmental conditions. For this research, a lab specimen, I-girder, concrete box-girder, and steel plate girder bridges were studied. A SHM system was installed on these structures and vibration and temperature data were collected. This data was used to understand how the bridge's natural frequencies typically change due to temperature.

17. Key Words	18. Distribution Statement
Dynamic Properties, Precast, Temperature, System Identification	

19. Security Classification (of this report)	20. Security Classification (of this page)	21. No. of Pages	22. Price
Unclassified	Unclassified	90	

Form DOT F 1700.7 (8-69)

ACKNOWLEDGMENTS

Thanks to the Utah Department of Transportation (UDOT), the California Department of Transportation (Caltrans), and the Long-Term Bridge Performance (LTBP) program without which this research wouldn't have been possible.

Navid Zolghadri, Marvin W. Halling, Paul J. Barr, and Nick Foust

Table of Contents

LIST OF FIGURES

LIST OF EQUATIONS

LIST OF TABLES

Chapter 1: Introduction

Context

Modal parameters are subjected to significant changes not only by damage, but also by environmental conditions. Without quantifying environmental effects, applying vibration-based damage detection techniques may result in false damage identification. Collecting vibration and temperature data continuously has enabled researchers to investigate the correlation between environmental effects and identified modal parameters. Amid different environmental effects, temperature variations have been found to have the biggest impact on vibrational characteristics of bridges.

This study addresses the effect of temperature on vibrational characteristics of three continuously monitored bridges and a lab specimen. The first bridge is a pre-cast I-girder concrete bridge located in Perry, Utah; the second is a concrete box-girder bridge in Sacramento, California; the third is a steel plate girder bridge in Salt Lake City, Utah. These bridges are instrumented with a monitoring system that collects vibration and temperature data at different locations on the bridges. The lab specimen is a 72 inch long steel plate instrumented with sensors and subjected to temperature changes.

Natural frequencies of the structures are identified from ambient vibration data using the Natural Excitation Technique (NExT) along with the Eigen System Realization (ERA) algorithm. Variability of identified natural frequencies was investigated based on statistical properties of identified frequencies. A linear autoregressive model with exogenous terms (ARX) and a nonlinear ARX model were used to find the relationship between the measured temperature and natural frequencies. The nonlinear ARX model showed natural frequencies are dependent on previously measured temperatures. This model was validated by using different

sets of available data. These two models were evaluated and compared based on statistical properties.

Scope and Organization

This report is organized into six chapters. A comprehensive literature review is presented in Chapter 2. Chapter 3 presents a detailed description of the studied structures. The location and physical characteristics of three bridges and a lab specimen used in this study are also described. Figures and plans show the number of spans, length of spans and cross-sectional dimensions. The location of installed sensors on each bridge is also described in detail. Chapter 4 describes the methods for identifying natural frequencies of the studied structures. Chapter 5 gives the statistical modeling steps used to create a base regression model to describe the temperature effects. Chapter 6 summarizes the study and its findings and provides conclusions.

Chapter 2: Literature Review

Influence of In-Service Environment on Modal Parameters (Alampalli, 1998)

This research is a study on SHM, which is referred to as remote bridge monitoring systems (RBMS) throughout this research paper. It brings to light that the bridge inspection and assessment process relies largely on visual inspection to detect bridge health or condition. It states that bridge owners are looking for more reliable tools to assist in inspection and assessment. The paper references other studies that have been successful in indicating damage through SHM. The paper also points out that, along with any other experimental techniques, SHM produces variable results when repeated. Causes for variability are listed as: test environment, electrical disturbance, in-service environment, and variation among operators. These causes for variability are also stated to cause as much variability in modal parameters as damage, as shown in referenced papers. The research and experiment of this study were focused on in-service environment and testing methods.

An experiment intended to capture the effects of in-service environment and testing methods, was established and conducted on a single-span bridge in New York. The bridge spans Mud Creek and consisted of two W18x64 beams which supported a reinforced concrete deck. The two W18x64 beams that spanned the creek were embedded in concrete abutments at each end. Damage was to be induced afeeter taking ten measurements of the modal parameters that would serve as the baseline of normal bridge behavior. Afeeter damage was induced, the modal parameters were measured again to compare to the baseline measurements. This study used only the natural frequencies of the bridge; the first three were selected. The air temperature was also measured at the same time the bridge frequencies were measured.

The baseline measurements were taken at the average temperature of 46.6°F, with the minimum temperature being 42°F. Afeeter the initial baseline measurements were taken, damage was induced, and twenty other measurements were taken. These twenty measurements were divided into two groups: (1) a group with temperatures well above freezing (32°F), and (2) another group with temperatures below or close to freezing. The results showed that the group well above freezing indicated a change in structural behavior since the modes all slightly decreased. The group with temperatures near freezing actually showed an increase of stiffness from the undamaged structure.

It was concluded that above freezing temperatures had no significant effect on the natural frequencies. The temperatures below freezing suggested a stiffening of the bridge which led to the belief that the supports were frozen and acted more fixed. It was concluded that the baseline should be established on at least one complete cycle on in-service conditions. These in-service environmental conditions should be well understood before establishing criteria to detect damage.

Comparative Study of Damage Identification Algorithms Applied to a Bridge: I. Experiment (Farrar and Jauregui, 1998)

This study covers the specific area within SHM of damage identification within civil structures. The paper presents the SHM goal of accessing civil structures, specifically detecting damage at the earliest stage possible. The authors list many methods that have already been developed, which do not fit within the SHM realm. These methods include: Ultrasonic, Acoustic, Magnetic Field, Radiography, Eddy-Current, and Thermal Field. The authors also give the limits of these methods. These methods require a knowledge that damage exists, an approximate location of the damage, the damaged area must be accessible and near the structure's surface.

SHM does not have these requirements, although it does have other demands that must be considered.

The goal to mitigate bridge failures is mentioned. The current process listed by the paper to monitor bridges and mitigate bridge failures is visual inspection techniques. It is stated that damage can occur between inspection intervals and that damage can go undetected during an inspection. The goal to mitigate bridge failures could fail because of the occurrences listed. The idea that the goal of bridge failure mitigation could be accomplished through constantly monitoring bridges with SHM systems might be appropriate since a major change in structural performance might be detected. This is an option as long as the methods and applications of SHM are fully understood and accepted.

Within the focused area of damage detection, the research paper gives the four levels of damage detection. These include four levels: (1) identifying that damage has occurred; (2) identifying that damage has occurred and its location(s); (3) identifying that damage has occurred, its location(s), and an estimation of severity; (4) identifying that damage has occurred, its location(s), an estimation of severity, and a determination of the remaining useful life of the structure. As of the time of this study, the limitations to which SHM can be used in these levels were not fully known. The variables that are used in SHM principles to fulfill these damage detection levels are the structure's natural frequencies, the mode shapes, and modal damping. These properties are functions of mass, damping, stiffness and boundary conditions.

In order to further understand SHM, an experiment was performed on the Interstate-40 (I-40) bridge in New Mexico. The intention of the experiment was to show the changes to the structure's natural frequencies, mode shapes, and modal damping due to damage that simulated fatigue cracking, which is common to plate-girder bridges. The steel plate bridge consisted of a

three-span, continuous, steel girder configuration that supports a concrete deck. A thermal expansion joint was located at both ends of the three-span bridge, one at an abutment and the other at a pier. Four levels of damage were induced to the bridge incrementally from light to heavy damage. The damage was in the form of different size cuts to the web of the north plate girder. The excitation, data acquisition system, and the parameters used in each are described. The damage influences to the natural frequencies were not noticeable until the worst case scenario. The structure's first three natural frequencies changed from 2.48, 2.96, and 3.50 hertz to 2.30, 2.84, 3.49 hertz, respectively, when bottom flange was finally cut in the worst case scenario. In the previous scenario, the natural frequencies were measured to be 2.46, 2.95, and 3.48 hertz. The only other modal variable reported, damping percentages, did not show any connection to the scenarios. This showed that the changes in the natural frequencies due to the prescribed damage was either being masked by other variables or not noticeable until the damage was more significant.

The authors concluded that the boundary conditions must be taken into account in the study and that linearity of the structure should be checked to some degree. The following needs are also mentioned in the paper: more sophisticated methods to examine modal data for indications of damage and the quantification of environmental effects on the measured modal properties through statistical analysis.

A Review of Structural Health Monitoring Literature 1996-2001 (Sohn et al., 2004)

An overall view of the topics within SHM is given by this paper. This paper focuses on SHM within structural engineering in the years between 1996 and 2001. The review first, describes the purpose and definition of SHM. It then, divides SHM into four categories with

specific topics within these categories. These topics are listed and discussed giving specific literature examples. Strong and weak points within these topics are listed. The review also gives specific direction that could bring progress to SHM in some of these topics.

Structural Health Monitoring is defined as "the process of implementing a damage detection strategy for aerospace, civil and mechanical engineering infrastructure" (Sohn et al., 2004). The authors explain that SHM monitoring is a statistical pattern recognition problem. Statistical pattern recognition models can be described by four categories including: (1) Operational Evaluation; (2) Data Acquisition, Fusion and Cleansing; (3) Feature Extraction and Information Condensation; and (4) Statistical Model Development for Feature Discrimination. These four categories and their respective topics are discussed independently below.

The paper lists four questions to explain the topics within the Operational Evaluation category. First, how damage is defined for the civil structure? Second, what operational and environmental conditions are present? Third, what limitations are caused by these conditions? Fourth, what are the economic or life safety reasons behind performing SHM? The studies within the selected year range were mostly laboratory tests. In these tests, operational or environmental variability is small. Economic or life safety considerations are not shown within these laboratory tests. The majority of these laboratory tests prescribe specific damage versus quantifying damage that is inflicted by the constant operational and environmental conditions.

The category of Data Acquisition, Fusion and Cleansing has the following topics: (1) selecting the type, number, and locations of sensors; (2) the data acquisition, storage, and transmittal hardware; (3) how long and ofeeten should measurements be taken; and (4) what techniques are used in filtering, cleansing, and fusion.

Feature extraction is noted to receive the most attention in literature. Finding structure properties used to distinguish between an undamaged and damaged structure is the process of feature extraction. Information condensation is the process of compressing the data collected into smaller amounts of data that are still usable in detecting damage. Data fusion is somewhat related and can be seen as a form of information condensation. The category of Feature Extraction and Information Condensation describe the main damage-sensitive properties as resonant frequencies, mode shapes, or properties derived from mode shapes. The paper states that investigators from the chosen time period are using system features transitioning from a time-invariant, linear system to a time varying, non-linear system as a result of damage.

The last category described in the literature review is Statistical Model Development. This category is noted to have received the least attention in the current and past reviews. Supervised learning is a type of algorithm that includes readings from the undamaged and damaged structure. Unsupervised learning algorithms include readings from the undamaged structure only. Unsupervised learning is said to be effective for identifying the onset of damage. Supervised learning is used more to find the location of damage.

It is concluded that two main problems need to be addressed: (1) the performance and validation of statistical techniques in real operational environments; and (2) the system's sensitivity to environmental and operational conditions that may be present.

Structural Health Monitoring of Civil Infrastructure (Brownjohn, 2007)

The topic of SHM is introduced as a developing but useful tool for inspection and assessment of structures. The paper was written to describe the motivations for SHM more in certain areas of civil infrastructure. SHM receives less attention within residential and commercial structures due to potential obligations and consequences if an owner were to know

the poor health or performance of their structure. Industrial or structures that support a business or public safety are considered higher risks and more research has been done in these areas due to the need and funding. Every structure within civil engineering is unique and could require special training, which can be expensive, to establish the normal or baseline performance of a structure. In other SHM fields, common rules can be prescribed, which is less expensive and tends to be more utilized. In order to focus on applicable topics this paper covers for the thesis topic, the following sections will be described: (1) the objectives of monitoring; (2) the history and motives of SHM in bridges and buildings; (3) the case study of the Tuas Second Link bridge; and (4) the present directions in civil SHM.

The main research objective for SHM within the civil field is the optimization process. With every structure being unique, the requirement of special and expensive training to apply SHM principles to view the structural health exists. The main aim of research is to develop effective and reliable ways to acquire, manage, integrate, and interpret structural performance data in order to get the maximum amount of information for the lowest cost. Removing the subjective human element from getting reliable health performance information would lower the cost.

The history and motives of SHM in bridges and buildings described by this paper include some of the earliest instances of monitoring. These earlier instances, Carder (Carder, 1937) and the University of Washington (University of Washington, 1954), were mainly motivated to document dynamic behavior. These monitoring programs or studies took record of the Golden Gate and Bay bridges along with the Tacoma Narrows Bridge, respectively. Studies have mainly focused on larger, more important lifeline structures. This paper gives SHM as a more beneficial tool for short-span highway bridges since global response changes can be seen without visual

inspection. For buildings, SHM has served more purposes than structural performance. SHM systems have been used for understanding earthquake and wind loadings more accurately. In both bridges and buildings, SHM data can be used to update, verify, and validate finite element models and their readings.

This paper gives a case study of a large span suspension bridge and a concrete box girder bridge. In order to summarize the applicable topics to the thesis topic, only the case study concerning the concrete box girder bridge is described. The Tuas Second Link Bridge was opened in 1998. During the construction of this bridge, a SHM system was installed. Strain gauges, accelerometers, and thermocouples were installed. This case study was chosen to be described since the bridge was a concrete box girder bridge along with the location of the thermocouples. The thermocouples could be used to find the temperature gradient. Although the bridge type and sensor locations were similar to the thesis project, the case study mainly focused on the strain readings and structural changes that occurred through the bridge's construction phases. Temperature was also found to be an important factor through different processes. The case study was shown mainly to show an example of the usefulness of SHM systems to give a motivation for SHM systems.

Present directions for SHM include sensors, data storage, data transmission, database management leading to feature extraction, data mining, load/effect model development from study of data, learning from past experience, and decision making from SHM data and models. The present thesis topic deals with many of the described directions this paper presents.

Environmental Variability of Modal Properties (Cornwell et al., 1999)

This study covers SHM and in particular a certain variable that affects at least one known modal property: temperature. Within civil engineering, SHM can be used to assess or evaluate

the performance or health of a civil structure. SHM assessment varies from visual or experimental. Civil structures are unique and research is aiming to optimize SHM systems, both the equipment and procedures used throughout the SHM process. SHM depends on measuring and evaluating the modal parameters. Three common modal parameters are described to be: resonant frequencies, mode shapes, and modal damping. Changes in these dynamic parameters could indicate a change in stiffness, damping, mass, or loading. This research shows that there are other important variables that must be taken into consideration in order to assess a structure's performance. The research focuses in on the environmental effects of temperature.

The experiment that was conducted to show the effects of temperature was performed on the Alamosa Canyon Bridge. This bridge is a seven-span, simply-supported, reinforced concrete beam bridge. The experiment was conducted on the first span of the bridge. A total of 30 accelerometers were placed in a grid-like fashion over the span, 58 inches apart in the direction of the bridge width and 76 to 98 inches apart in the direction of the bridge length. All thermometers were located at the mid-span at the following locations: one on the bottom of the concrete deck at center width, two on the exterior web of the outside girder, and two on the top of the concrete deck above the exterior girder. Expansion of the bridge was limited by dirt inside the expansion joints.

The experiment took a total of 24 hours. A total of 30 averages were used to take the frequency measurements every two hours, which took about 30 to 45 minutes to complete. The average temperature readings were also taken for these time periods. The correlations between the following temperature readings and the resonant frequencies were compared: individual temperature measurements, average temperature at the top and bottom of the deck, and temperature differences from the east and west sides of the bridge. The highest correlation factor

came to be 0.94 and was obtained by the temperature differences from each side of the bridge. The first three resonant frequencies varied by 4.7 percent, 6.6 percent, and 5.0 percent, respectively, over this day. This experiment indicates that another important variable that affects modal parameters is temperature or temperature gradients. It was noted that a similar correlation obtained could also be obtained by using a time-shifeeted analysis. This is due to frequency changes lagging behind temperature changes.

The findings of this study indicate that the temperature differential across the deck correlated with the resonant frequencies the best. The need to understand the principles behind the effects of temperature in modal parameters is explained. The development for procedures and processes to filter out temperature effects in structural assessment is necessary.

Damage Detection Accommodating Varying Environmental Conditions (Giraldo et al., 2006)

This study covers the specific area within SHM of identifying and locating damage or a loss of stiffness in a lab created building structure. This is accomplished with temperature effects being considered. The evidence of the increasing need to effectively, economically, and efficiently assess many civil structures with the increase of quantity and complexity is described. An example of the city of Seattle, that has over 150 bridges, needing an overall infrastructure assessment afeeter a major event, such as an earthquake, is given. It mentions that SHM is of major interest for assessment purposes and that many studies are being conducted in order to simplify the process for the application in the civil engineering field. Within this field, each structure is unique and the process to apply SHM is very specialized and expensive. The results of a study are presented in this paper.

The proposed technique to use SHM as an assessment tool utilized the following analyses to identify the existence and location of damage: Natural Excitation Technique (NExT), Eigen system Realization Algorithm (ERA), and a nonlinear principal component analysis (NL-PCA). The NExT and ERA analyses are used for modal identification. Stiffness identification is then used by selecting an appropriate identification model (ID-model), which limits the capabilities of SHM techniques applications. These models typically simplify the structural dynamic response. PCA is then completed and the residual error as a percentile reduction in element stiffness rather than the absolute value is used to indicate damage. An advantage of this proposed technique is that the residual error change is independent of the environmental factors. The limitation that this method will not give the extent of damage is mentioned. These analyses are further described in the paper.

A brief example of a two element structure is given. The PCA of this structure is shown graphically and an example of how the residual error is used to determine stiffness losses in one of the elements. Once this is described, an example of an outlier analysis is shown for this specific example to set the criteria for damage alert.

Finally, a numerical example on a four-story experimental building is given. A finite element model of the actual structure was used to produce ambient vibration responses. Ambient vibration, sensor noise, and varying environmental factors were simulated. An appropriate ID-model was developed and the analyses were performed. Eight damage cases were utilized to simulate the response of the system and compare to the undamaged case. This technique resulted in indicating the correct elements had lost stiffness in five of the eight cases. The other three cases, false negatives were indicated; although in one of these cases, a false positive was accompanied by correctly identifying one element that had lost stiffness.

The paper concluded that the residual error was successfully used as a damage indicator. It mentions that the approach used is limited to cases where stiffness losses effect the dynamic properties. It is also mentioned that this approach could be limited to structures that do not experience stress stiffening of members due to thermal expansion since the test specimen was free-standing.

Temperature Effect on Vibration Properties of Civil Structures: a Literature Review and Case Studies (Xia et al., 2012)

This paper introduces SHM and how it can be used in condition assessment, specifically for civil structures. It also, describes many studies that give examples of existing problems within SHM, mainly variations in vibration properties due to temperature effects. These effects are shown to be in most civil structures including bridges, buildings, and laboratory experiments. The paper describes different statistical models used to relate these effects. Afeeter, it gives a quantitative analysis, laboratory comparative study, and two case studies. It was concluded that variations in frequencies are mainly cause by material changes in the modulus under different temperatures.

This paper summarizes many of the results that studies have given that attempt to explain the temperature effect on vibrational properties. The paper introduces the topics of vibration-based structural condition assessment and SHM by describing some of the problems that structural temperature and environmental variations create. Results from multiple studies are referenced to show that temperature variations are shown to be as or more significant than structural damage. It is stated that if temperature effects are not taken into account, vibration-based condition assessment can be impacted. Other variables that play important roles in making

assessments more reliable are mentioned to be boundary condition changes, non-uniform temperature distributions, and thermal inertia effects.

This paper explains and refers to the findings from many papers that show how a structure's vibrational properties and temperature relate. Variations in natural frequencies, mode shape, and damping are how the vibrational properties are divided. The vibrational properties, in this same order, describe the extent to which the relationship to temperature is understood. The percentage change, if available, in each of these vibrational properties is given.

Afeeter the relationship between temperature and vibrational properties are described, the statistical models on modal frequencies are described. The models described include: regression models, autoregressive models, and principle component analysis. Within all three categories of statistical models and tools listed in this paper, the referenced papers were categorized into groups. These groups consisted of the following categories: linear regression and multiple linear regression models, control chart analysis, support vector machine technique, autoregressive (AR) and autoregressive with an exogenous (ARX) model, and principle component analysis.

A quantitative analysis was performed for this study. The analysis found that the percent change of the natural frequency of steel, aluminum, and reinforced concrete (RC) beams with temperature are 0.018, 0.028, and 0.15 percent per degree Celsius, respectively. These values are then used to compare with the results from the laboratory comparative study, case studies, and in the conclusion and discussion sections. In the laboratory comparative study, the percent change found for steel, aluminum, and RC beams were 0.036, 0.056, and 0.30 percent, respectively. Close to half of the variations in natural bending frequencies are shown to be from modulus changes due to temperature. No correlation between damping and temperature was found. The effects that temperature had on mode shapes were not covered by this paper.

Two case studies of the Tsing Ma Suspension Bridge and the Guangzhou New TV Tower were described in this paper. The suspension bridge had an average percent frequency change of 0.018 percent, which is close to that found for the steel beam. The TV Tower percent change was not listed, although the slope of the linear fitted curve was noted to be 1.5×10^{-3}/°C, which was close to half the concrete laboratory slope of -3.0×10^{-3}/°C. In conclusion of these case studies, the paper implied that even in a large-scale structure, variations in bending frequencies are mainly due to effects of modulus changes due to temperature.

The applicable conclusion of this paper that relates to the topic of interest is the following: the changes of natural frequencies seen in civil structure are mainly produced by material changes (modulus) under different temperatures.

Chapter 3: Lab Specimen and Bridge Descriptions

In this chapter, three things will be discussed. First, a detailed description of the studied bridges and the lab specimen is presented. Second, a description of the Structural Health Monitoring (SHM) system that is installed on the bridges and the lab specimen will be given. Finally, a typical sample of recorded data from these bridge structures will be presented.

Lab Specimen

A lab specimen, shown in Figure 1, was subjected to dynamic testing to study the effect of temperature on dynamic properties. This specimen was a steel beam with a rectangular cross section of 12 by 1 inches. The supports for this beam were two channel shaped that were flipped and placed on a frame with two columns with 4 by 4 inch box cross section (Figure 2). On the channel, a 4 by 4 inch angle was inverted and used for the support for the beam. This support condition was assumed to be pinned-roller. In order to increase the temperature, two heaters were used while this lab specimen was sheltered with a plastic cover (Figure 3).

Figure 1: Lab Specimen

Figure 2: Support Condition

Figure 3: Covered Lab Specimen (Temperature Tent)

Type-T thermocouples were used to measure temperature from different locations of the specimen. Figure 4 shows the location of installed thermocouples at 0.25L, 0.5L and 0.75L.

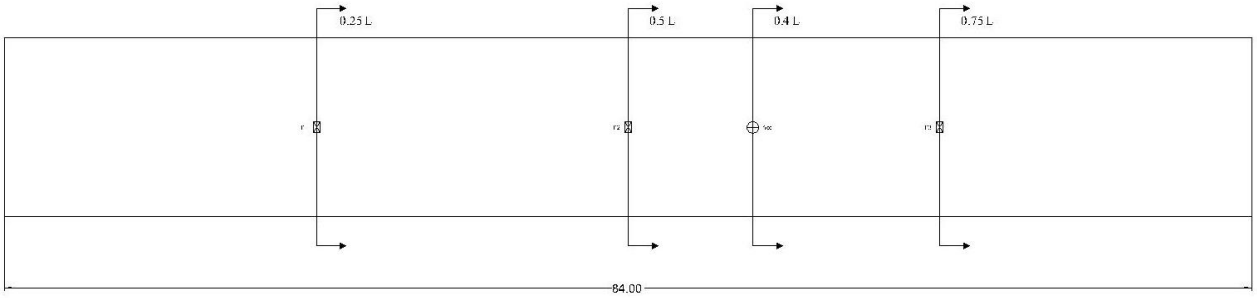

Figure 4: Plan View of the lab specimen

The Datalogger that was used to make measurements from thermocouples in this experiment was a CR6. The latest operating system was loaded to this datalogger, therefore it can communicate with a PC through a USB cable. The temperature was collected every 5 minute for this experiment. Dynamic data were collected with the Bridge Diagnostics Incorporated STS-WIFI system. The base station was connected to the computer which already had the BDI drivers installed. The data was recorded and the time of each test was mapped with the recorded data from the other data logger.

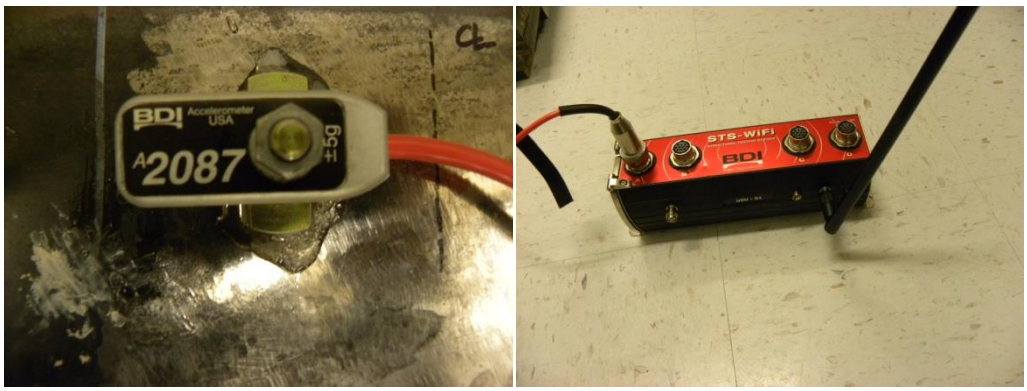

Figure 5: Accelerometer and STS Wifi Node

Afeeter turning the heaters on, the temperature of the lab specimen started rising (Figure 6). Dynamic testing was done every one hour for 11 hours. Impact excitation was used and

acceleration was recorded. As Figure 6 shows, the temperature fluctuates as the heaters turn on and off, but the variation in the temperature is not significant afeeterwards.

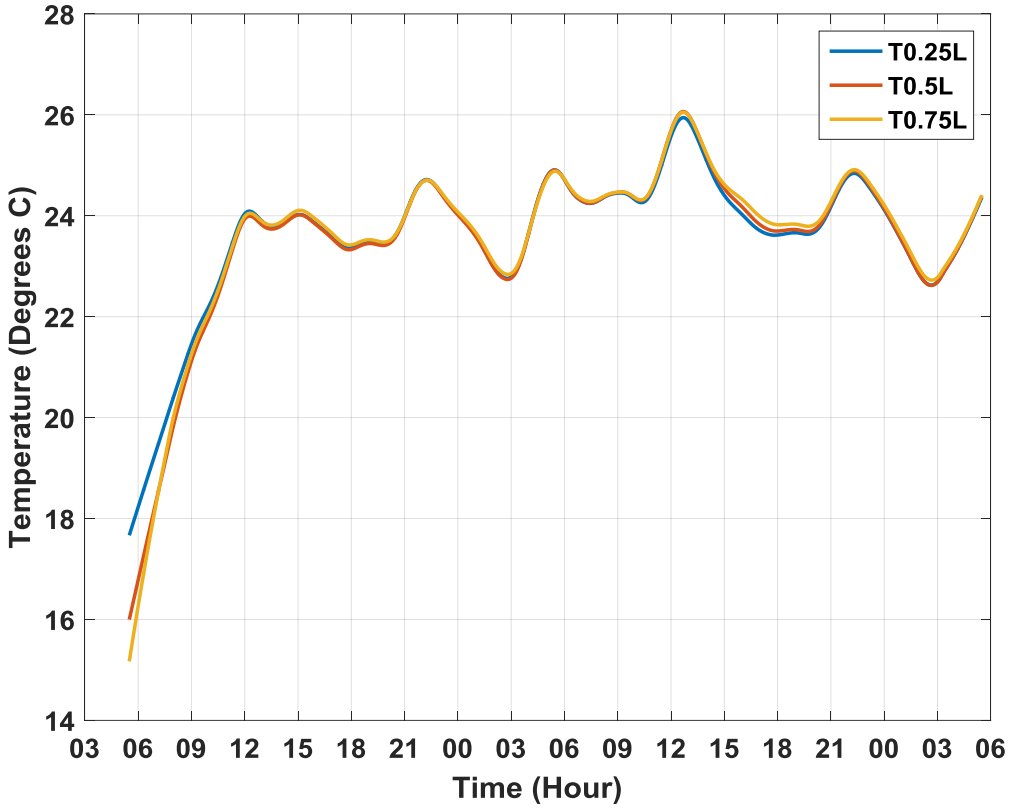

Figure 6: Temperature Variation of the Lab Specimen

Perry Bridge

The Cannery Street Overpass, is located in Perry, Utah. It is located 1.8 Km north of a port-of-entry station where all trucks are directed to pass over an in pavement WIM and some trucks must stop at the station (Figure 7). The bridge is a pre-cast, pre-stressed, simple-span concrete girder bridge. The clear span length is 24.38 m, from abutment to abutment, with an actual girder length of 24.88 m from center-of-bearing to center-of-bearing. The abutments were designed as integral abutments. The width of the bridge is 13.40 m with a 12.34 m wide traveling surface comprised of two 3.66 m wide traveling lanes, a 3.42 m shoulder on the east side, and a

1.6 m shoulder on the west side. Both parapets are 0.53 m wide. The five girders are spaced at 2.69 m center-to-center with the centerline of the first girder located at 1.32 m from the East edge of the bridge (Figure 8). The reinforced concrete deck is 20.32 cm thick with specified minimum compressive strength of 24 MPa. The deck is covered with a moisture barrier membrane and 7.6 to 8.9 cm thick asphalt overlay.

Various types of permanent, long term instrumentation were installed on or near the bridge. The locations of these measurement devices were determined afeeter live load and dynamic field testing had been performed. The long term instrumentation includes foil strain gauges, vibrating wire strain gauges, tiltmeters to measure rotation, velocity transducers, thermocouples, hydrotracker embeds, impedance sensors, Luffeet IRS21 for road surface conditions, Decagon 5TE for measuring water content in the deck, a weather station on a nearby tower and a camera mounted to the top of the tower.

A data acquisition box (Figure 9) is located at the bottom of the tower. This box contains two dataloggers to which all of the instruments are connected except the hydrotrackers, impedance sensors and in-pavement WIM. The hydrotrackers and impedance sensors require on-site collection and the WIM data is transmitted from the port-of-entry server directly to USU's offsite server. The two dataloggers are used to record, process and transmit data from the instruments to the offsite server for data archival and further analysis. The data is transmitted via a CDMA cellular modem to the server.

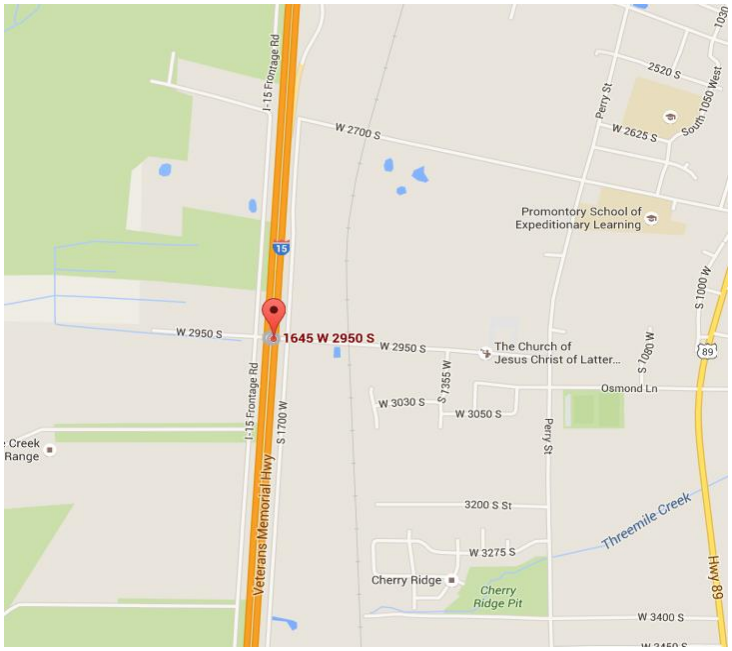

Figure 7: Bridge Location from Perry, Utah

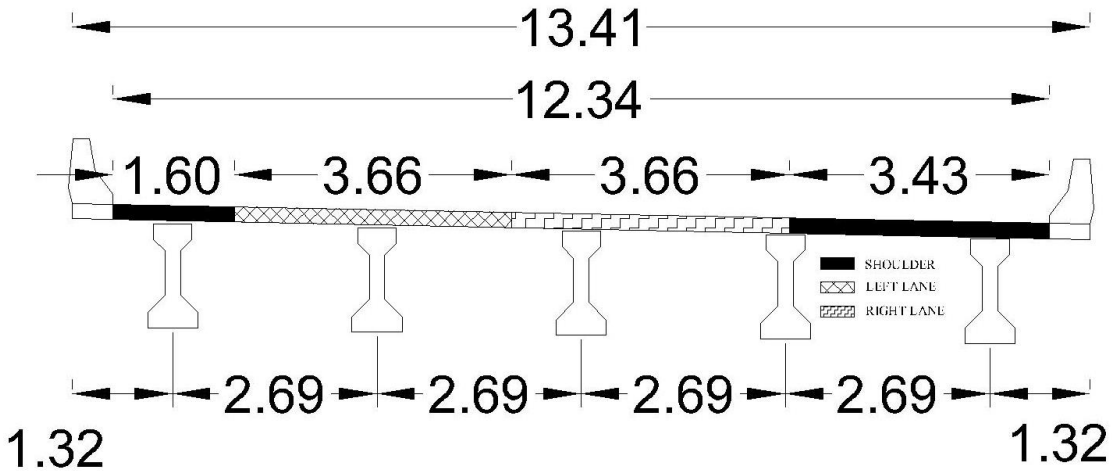

Figure 8: Cross Sectional View of Perry Bridge

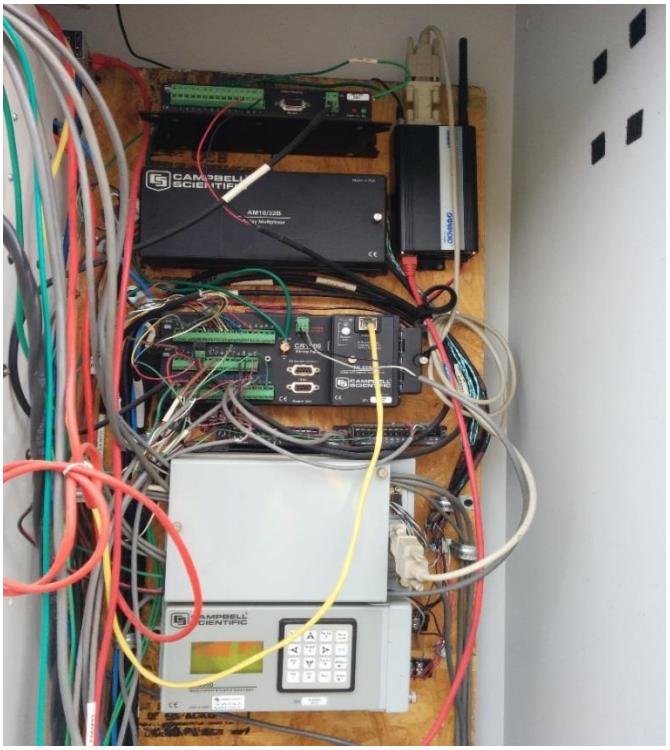

Figure 9: Data Acquisition Systems

The vibration of the bridge is measured by velocity transducers (VT1, VT2 and VT3) that are mounted at locations showed in Figure 10. Dynamic responses of the bridge structure to ambient excitations are recorded every hour for 3 minutes. These excitations include traffic load and environmental effects. The sampling frequency of the data acquisition recorder was set to 100 Hz and each set of data had (3*60*100=18000) samples. Thermocouples (T1-T5) are installed at selected locations on the girders (Figure 10). These installed thermocouples are placed next to the velocity transducers that are mounted in protective boxes under the deck. A weather station has been placed next to the bridge that is equipped with sensors to record wind direction, wind speed, radiation, humidity and air temperature. Environmental data are sampled every 3 minutes. Dataloggers are programmed to read and take an average of five measurements in order to smooth instantaneous errors in temperature measurements. The averaged value of the five temperature measurements will be saved and collected every 15 minutes. The data were

collected between January 1, 2015 and June 30, 2015 (181 days). On March 8, one collected hours is missing according to daylight saving time. Therefore, the total number of sets of data which were subjected to further analysis in this study was 181*24-1=4,343.

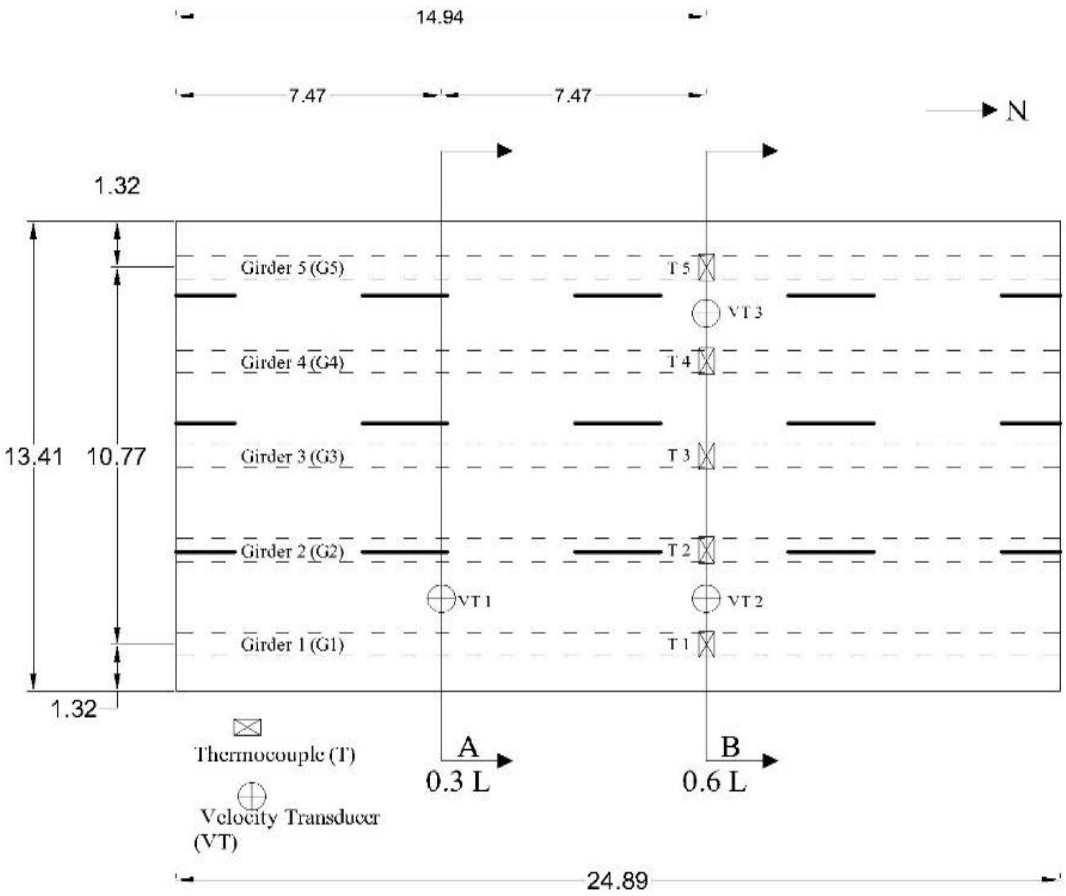

Figure 10: Sensors Layout

Figure 11 depicts a typical set of measured daily air temperature and temperature at Girder 1 (T1) to Girder 5 (T5). Girder 1 is on the east side of the bridge which is exposed to sunlight in the morning. In contrast, T5 is on the west side of the bridge. It can be seen in Figure 2 that the recorded temperature from T5 is higher than other temperature measurements in the afeeternoon because of its exposure to sunlight. The seasonal changes in temperature was

visualized in Figure 12 and mean and standard deviation of temperature have been summarized separately for each month in Table 1. The average air temperature measured from the weather station next to the bridge showed temperature changed 41 degrees Celsius (-9 to 31) in the first six months of 2015 while the changes in temperature measured on the girders is 27 degrees Celsius (0.32 to 27.79).

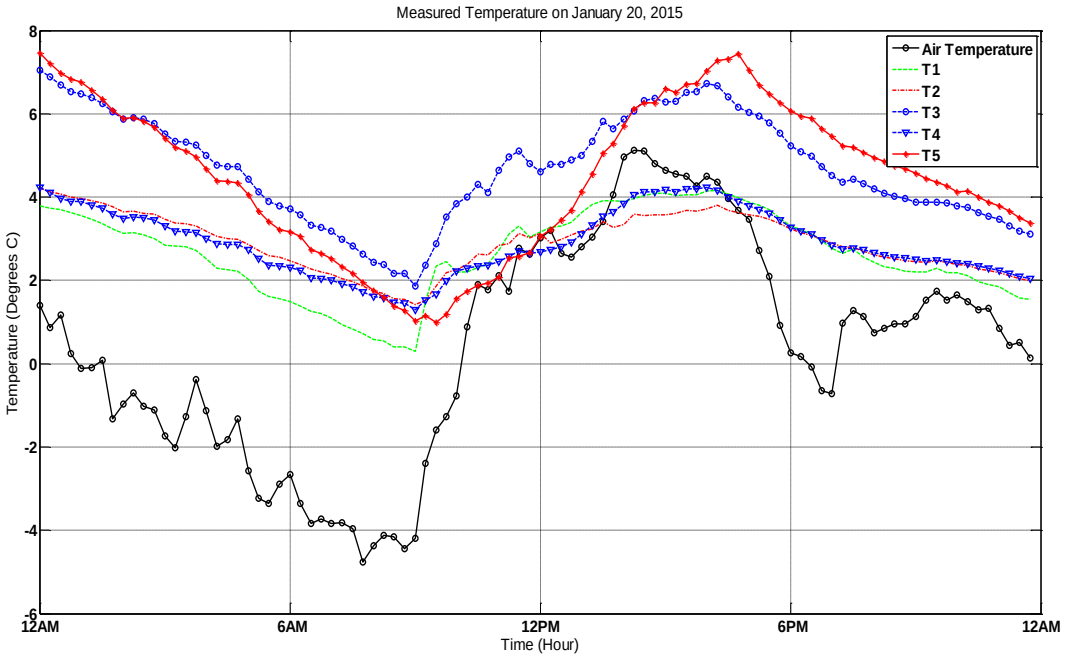

Figure 11: Daily Temperature Measurements (January 20, 2015)

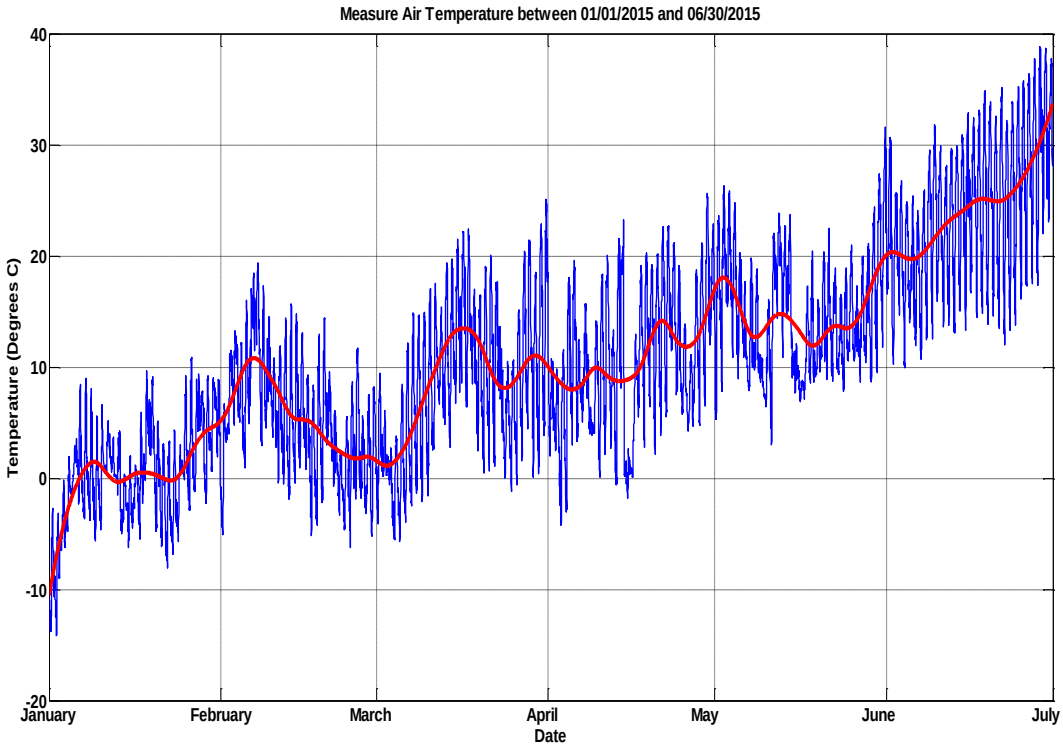

Figure 12: Temperature Trend from January 1 to June 30

Table 1: Monthly Mean and Standard Deviation of Temperature

		January	February	March	April	May	June
Air Temperature	Mean	0.32	5.57	8.72	10.62	14.71	24.21
	STD	4.51	5.24	6.63	6.14	5.00	6.59
T1	Mean	1.10	7.09	10.91	13.22	16.77	27.34
	STD	3.47	3.65	4.97	4.57	4.14	4.46
T2	Mean	1.08	7.08	10.68	13.06	16.59	26.95
	STD	3.33	3.42	4.66	4.10	3.70	3.98
T3	Mean	1.16	7.09	10.67	13.05	16.59	26.90
	STD	3.34	3.45	4.70	4.13	3.69	4.03
T4	Mean	1.21	7.13	10.75	13.16	16.75	27.15
	STD	3.36	3.51	4.80	4.26	3.81	4.21
T5	Mean	1.34	7.31	11.09	13.54	17.13	27.79
	STD	3.43	3.63	4.99	4.59	4.06	4.44

California Lambert Road Bridge Description

The Lambert Road Bridge was built in 1975 and located approximately 20 miles south of Sacramento. The bridge takes Interstate-5 (I-5) southbound traffic over Lambert Road. Two traffic lanes are carried by this cast-in-place, four-cell, box-girder concrete bridge. This double-span bridge measures a total length of 78.64 m (258 feet). It is supported by a bent cap and column, such that each span measures a length of 39.32 m (129 feet). The bride spans in the North-South direction and has an 8° skew with each supporting abutment and the centered bent cap. Figure 13 shows the location of the Lambert Road Bridge relative to Sacramento, taken using Google Maps. Figure 14 shows a plan view taken using Google Maps, while Figure 20 shows a plan view with the dimensions labeled. Figure 15 shows an elevation looking east of the lambert road bridge.

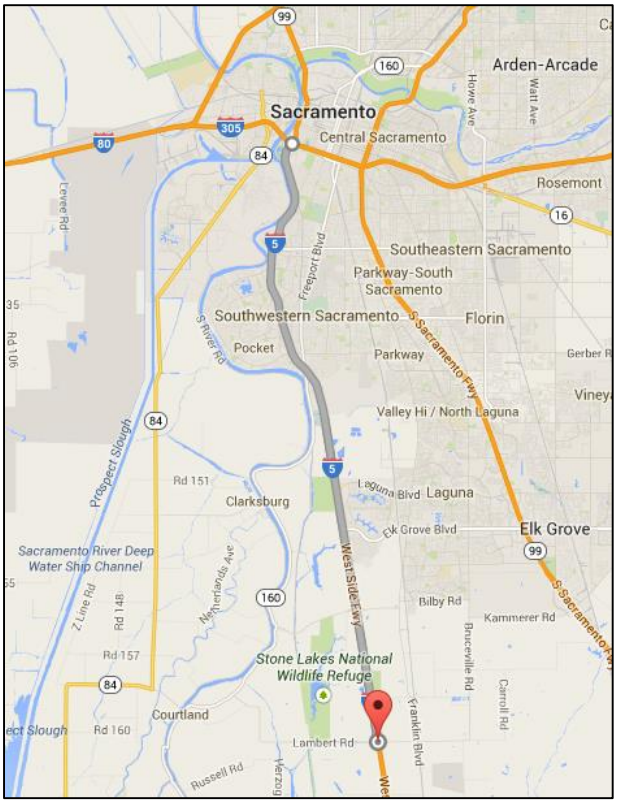

Figure 13: Bridge Location from Sacramento, California (Google Maps, 2014)

The Lambert Road Bridge is a box-girder design that measures a total width of 12.8 m (42 feet) and a road width of 12.2 m (40 feet). This road width carries two 3.66 m (12 feet) traffic lanes and the east and west shoulders that measure 3.05 (10 feet) and 1.83 m (6 feet), respectively. The two surrounding barriers measuring 0.3 m (1 foot) make the difference between the total width and the roadway width.

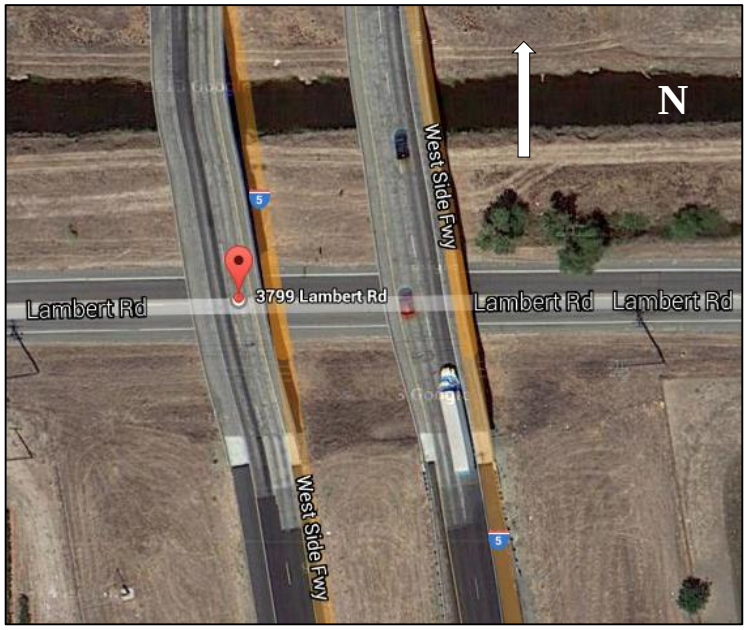

Figure 14: Satellite Plan View

Figure 15: Elevation Looking East

Structurally, this bridge is a four-cell, box-girder design. The average deck thickness measures 200 mm (8 in.). The deck overhangs the box-girder cells a distance of 0.92 m (3 feet). The bottom of the box-girder, or the bottom flange, is on average 150 mm (6 in.) thick. The five girders, or webs, connecting the deck and the bottom flange are each 0.30 m (1 foot) thick. The outermost girders are inclined from vertical by 30° and make the two outermost cells trapezoidal. The bottommost part of the trapezoidal cells measure 1.58 m (5 feet-2 in.) from wall-to-wall. The

two most inner cells measure 2.44 m (8 feet) in wall-to-wall width. All four cells measure 1.32 m (4 feet-4 in.) in wall-to-wall height, which makes the total height of the box-girder 1.68 m (5 feet-6 in.). Figure 16 shows a typical cross-section view of the box-girder bridge.

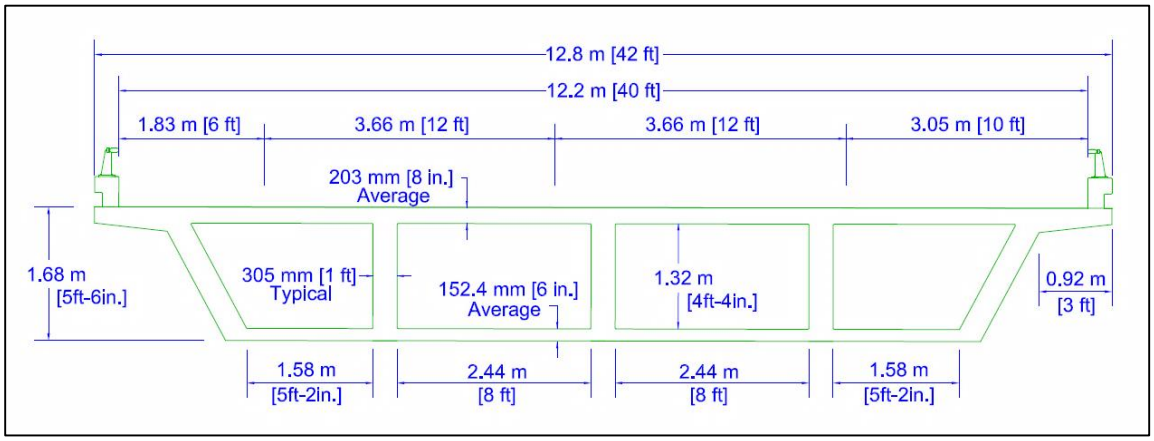

Figure 16: Typical Cross-Section

There are three diaphragms located on the deck; a 1.83 m (6feet) thick intermediate diaphragm at the bent cap and two 203 mm (8 in.) thick diaphragms at each midspan. These reinforced concrete diaphragms have a similar 8° skew as the abutments. The bent cap is supported by a bent column that measures 1.07 m (3 feet-6 in.) wide. The supporting column tapers at a 14-to-1 slope outwards (east and west) when moving upward from the ground to the bent cap. The column foundation measures 5.48 m by 3.66 m (18 feet by 12 feet) and 1.07 m (3.5 feet) thick. Each girder was prestressed with strands that followed a parabolic path. Figure 17 shows an elevation view of the bent cap and column (Hodson, 2010). Figure 18 shows a section cut of the column (Hodson, 2010).

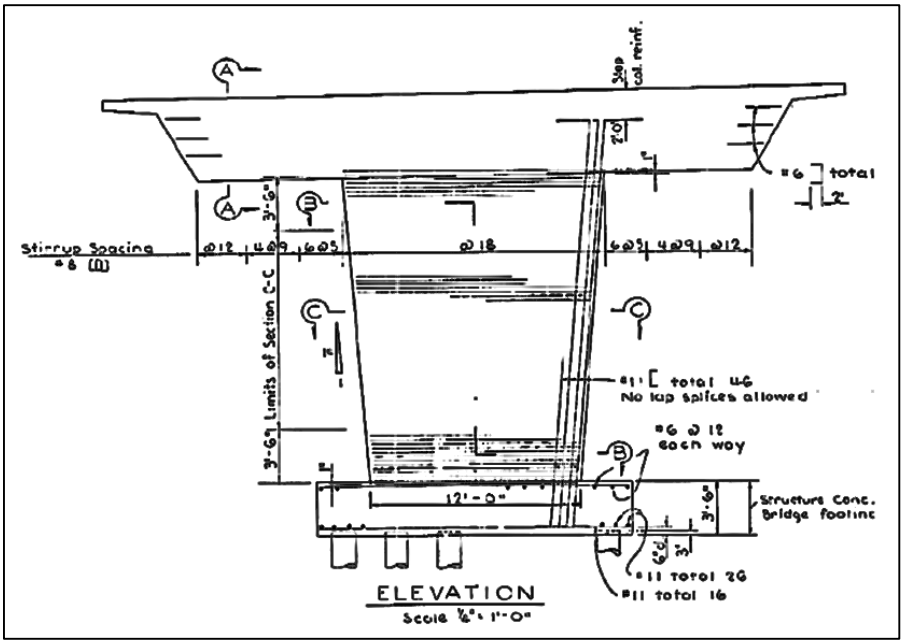

Figure 17: Bent Cap & Column Elevation (Hodson, 2010)

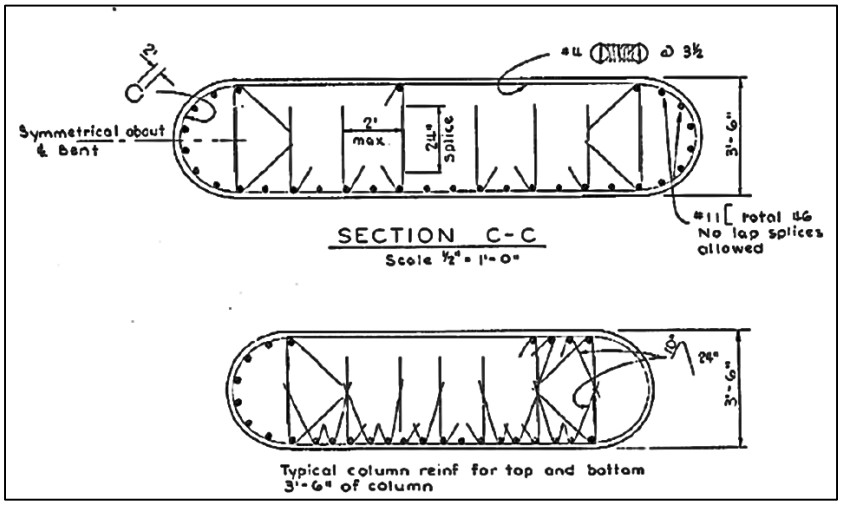

Figure 18: Column Section (Hodson, 2010)

The ends of the box-girder bridge are supported by integral abutments with wing walls attached. The abutments are 0.46 m (1.5 feet) thick and are supported by a reinforced pile cap, between which is a neoprene bearing pad. The pile caps measure 0.46 m (1 foot-6 in.) thick by 1.22 m (4 feet) wide by 12.96 m (42.5 feet) long. Each pile cap is supported by seven 406.4 mm

(16 in) diameter, cast-in-drilled-hole, concrete piles. The design loading of the piles is 623 kN (70 tons). Figure 19 shows the abutment detail (Hodson, 2010).

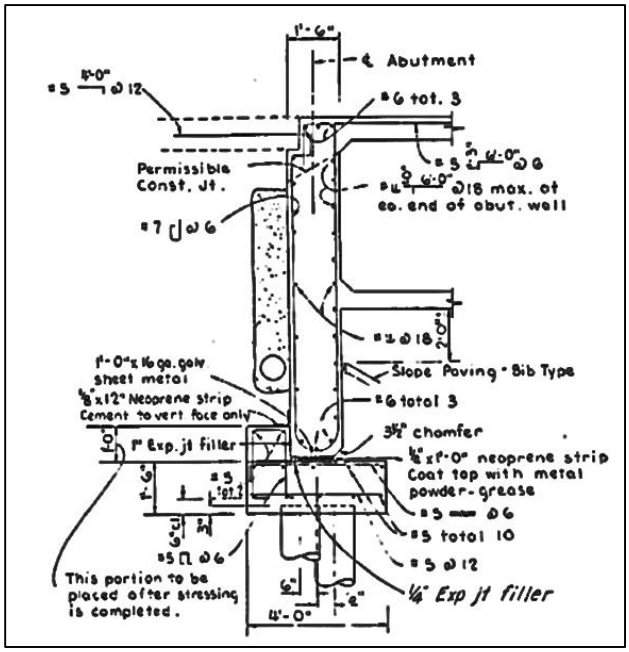

Figure 19: Abutment Detail (Hodson, 2010)

A structural health monitoring (SHM) system was installed on the Lambert Road Bridge. Two Campbell Scientific Dataloggers, a CR1000 and a CR5000, were utilized as the data acquisition systems. The SHM system has been recording the bridge response and certain environmental conditions since May 2011. Seventy-one sensors were installed and include the following: 16 Hitec strain gauges, 4 Geokon vibrating-wire strain gauges, 4 Mark Sercel velocity transducers (geophones), 3 Geokon tiltmeters, and 44 Omega thermocouples.

Since the SHM had started recording, the sampling rates and recording times have changed numerous times. The following recording descriptions are for the data used through this study and neglect records sampled under other conditions. The records can be categorized into two groups based on their sample rates. The velocity transducers, tiltmeters, and 12 of the Hitec strain gauges had a sampling rate of 50 hertz, which is grouped into the "fast sampling rate"

category, which takes a 5 minute data burst of records. Every sensor, except the velocity transducers, also took a measurement every 15 minutes, which is grouped into the "slow sampling rate" category. The tiltmeters also measured its own temperature and records this value every 15 minutes. The recordings in both the fast and slow sampling rate categories are recorded for further understanding of the bridge behavior throughout the structure's lifespan.

In order to give the locations of the sensors, named section cuts are made through the bridge. These sections follow the 8° skew that the abutment and bent cap established. A plan view with the section cuts is shown in Figure 20. Section A-A and Section H-H correspond respectively to the north and south abutment. Section D-D corresponds to the longitudinal center of the bridge. A length of L = 39.32 m (129 feet) is noted for the two spans. This same L is used to describe the spacing between the section cuts. The distance measured from Section A-A to Section B-B is 0.30L. From Section B-B to Section C-C measures 0.30L. From Section C-C to Section D-D measures 0.40L. This same spacing is used for the south span when respectively measuring to Sections F-F, G-G, and H-H from the Section D-D. Section E-E is 2.41 m (7 feet-11 in.) south of Section D-D. All sensors are located on, or close to, these sections. Table 2 summarizes the sensor location and names.

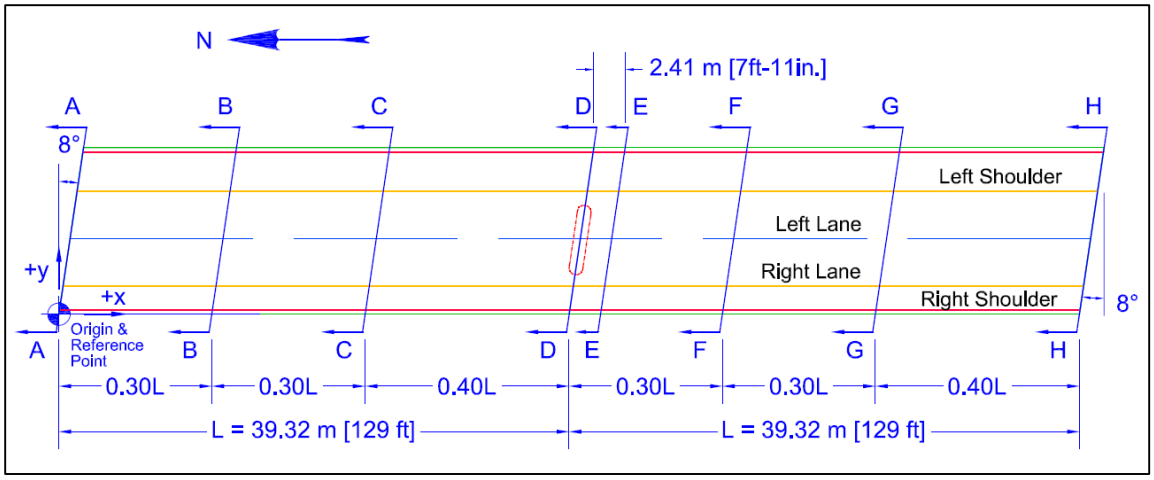

Figure 20: Plan View with Sections

The longitudinal locations are given by the sections. The transverse and depth locations are now given. The transverse dimensions are always given from the west side of the bridge and the depth locations are measured from the top-of-deck surface. Sections A-A, D-D, and H-H have tiltmeters located at the transverse location of 5.03 m (16 feet-6 in.) and at a depth of 508 mm (1 foot-8 in.). The tiltmeter names and locations in Table 2 correspond to Figure 21.

Sections B-B and F-F have a velocity transducer and two Hitech strain gauges paired at the same location as two thermocouples. At these two sections, the velocity transducers are located at the transverse direction of 5.03 m (16 feet-6 in.) right below the deck, a depth of 152 mm (6 in.). Both sensor pairs of the strain gauge and thermocouple are located transversely at 6.4 m (21 feet). The depth locations of these pairs are 460 mm (1 foot-6 in.) and 1680 mm (5 feet-6 in). These sections and the sensor names corresponding to Table 2 are shown in Figure 22.

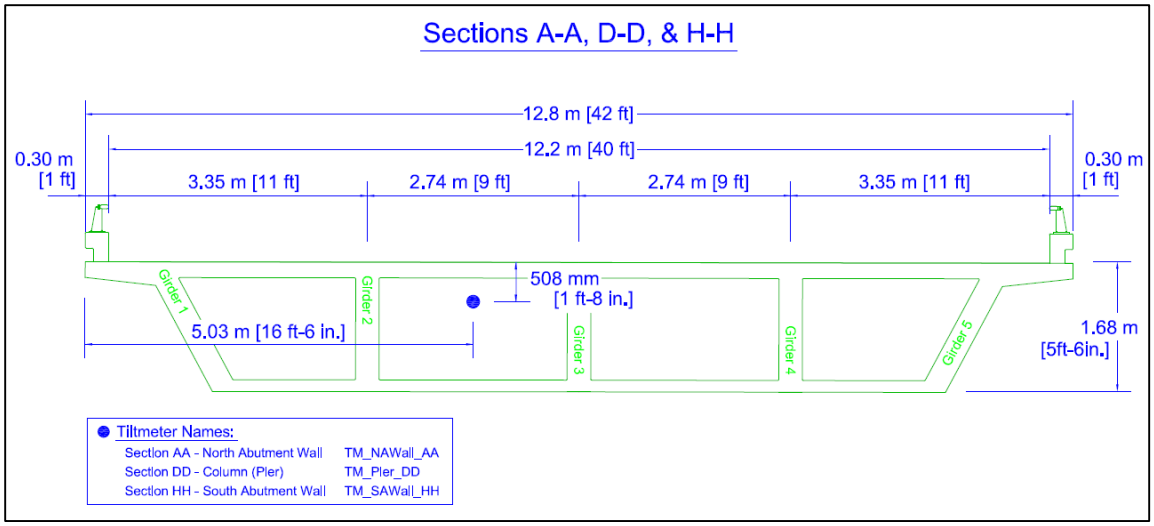

Figure 21: Tiltmeters at Sections A-A, D-D, & H-H

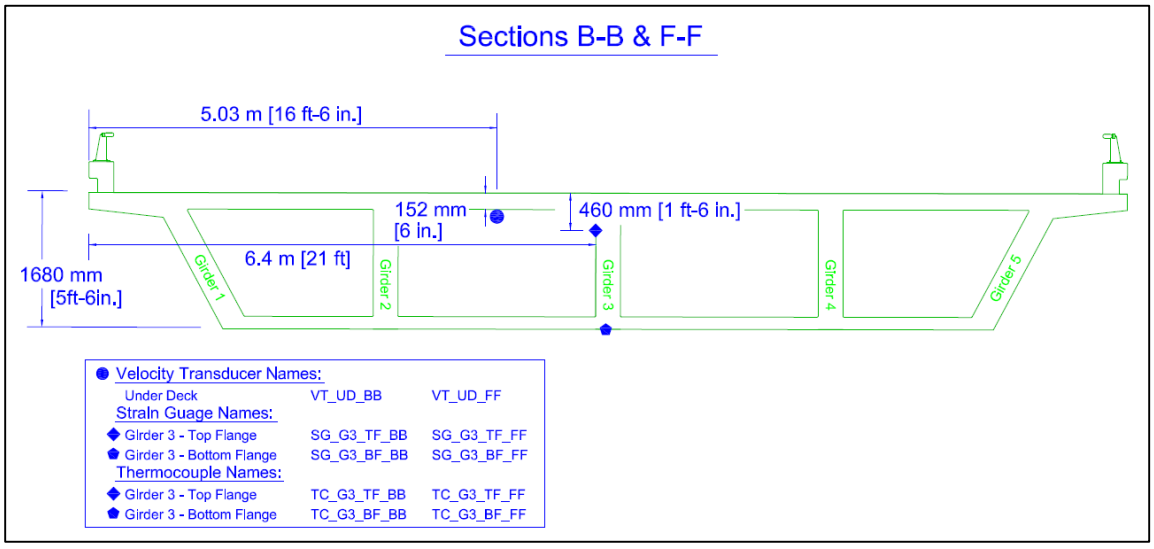

Figure 22: Sensor Locations at Section B-B & F-F

Sections C-C and G-G have a velocity transducer and six groupings of other sensors. These sensor groupings contain a mixture of Hitech strain gauges, vibrating wire strain gauges, and thermocouples. The transverse and depth locations of these pairings are explained solely in Table 2 due to their various locations. The velocity transducers at these two sections are located at the same transverse and depth locations as in Sections B-B and F-F, 5.03 m (16 feet-6

in.) and 152 mm (6 in.), respectively. These sensor names and some locations are also labeled in Figure 23.

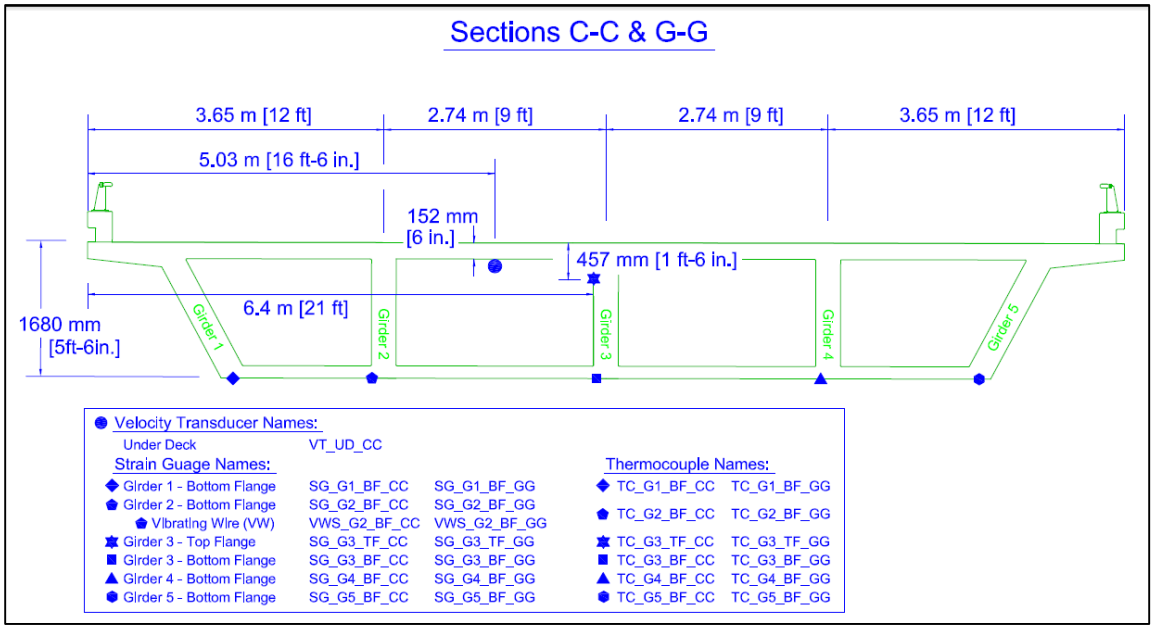

Figure 23: Sensor Locations at Sections C-C & G-G

Section E-E has the other 30 thermocouples. These thermocouples can be divided into two groups intended to measure the temperatures through the depth of the bridge. They measure the temperatures at different depths of the bridge to understand the bridge temperature gradient. The west group is situated transversely at 1.57 m (5 feet-2 in.), while the east group is at 3.10 m (10 feet-2 in.). The five, lower, web thermocouples of the west group are not exactly at this transverse location, due to the angle of the outermost box-girder wall, but Table 2 gives these exact locations. The web thermocouples of the east group are at a transverse location of 3.51 m (11 feet- 6 in.). The depths and configuration of the ten deck thermocouples of each group is given in Figure 24.

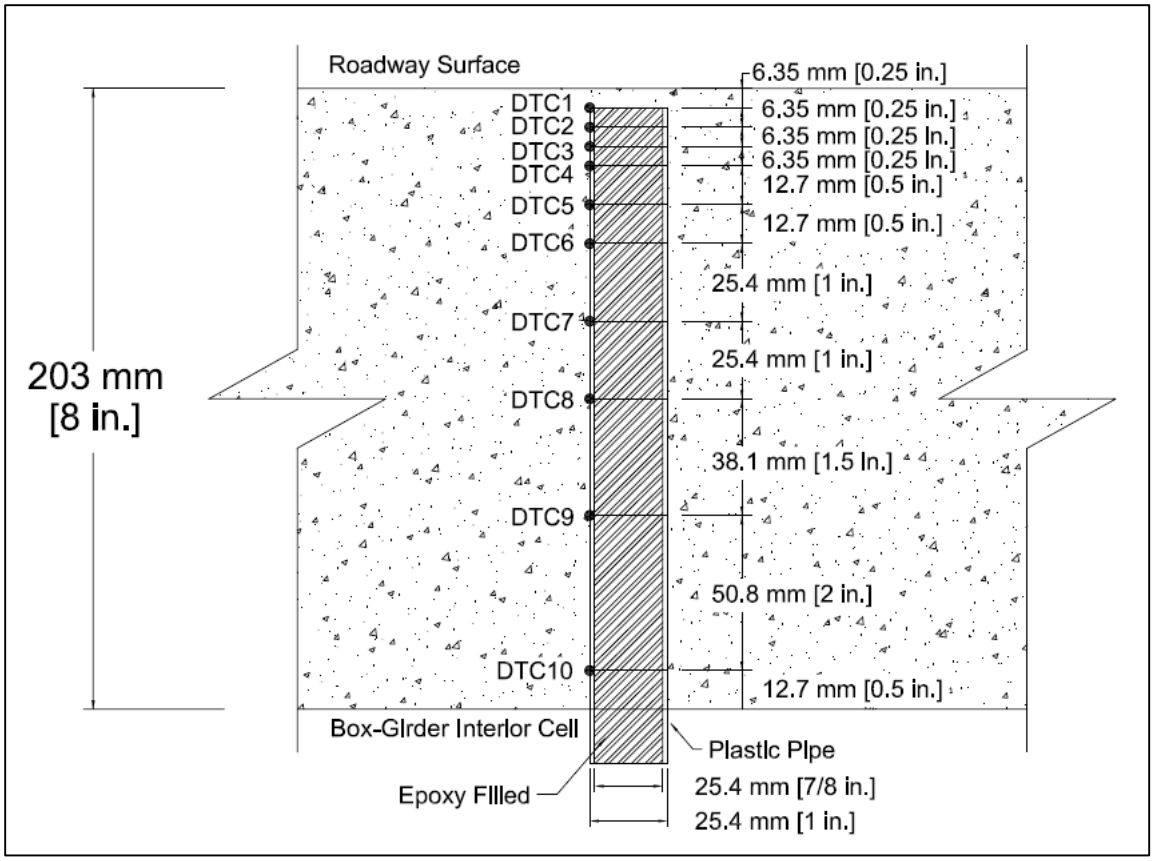

Figure 24: Deck Thermocouple (DTC) Locations

The deck thermocouples are actually located inside the deck. When the SHM system was installed, a hole was bored most the way through the deck from within the box-girder cells. The deck thermocouples were distributed through a plastic pipe which was placed within this hole through the deck. The plastic pipe was then epoxied in place and filled with more epoxy. The lower web thermocouples were epoxied to the box-girder bridge as closely to the transverse location of the deck thermocouples. The depths of the web thermocouples of both the east and west groups are also in Table 2. Section EE is shown in Figure 25.

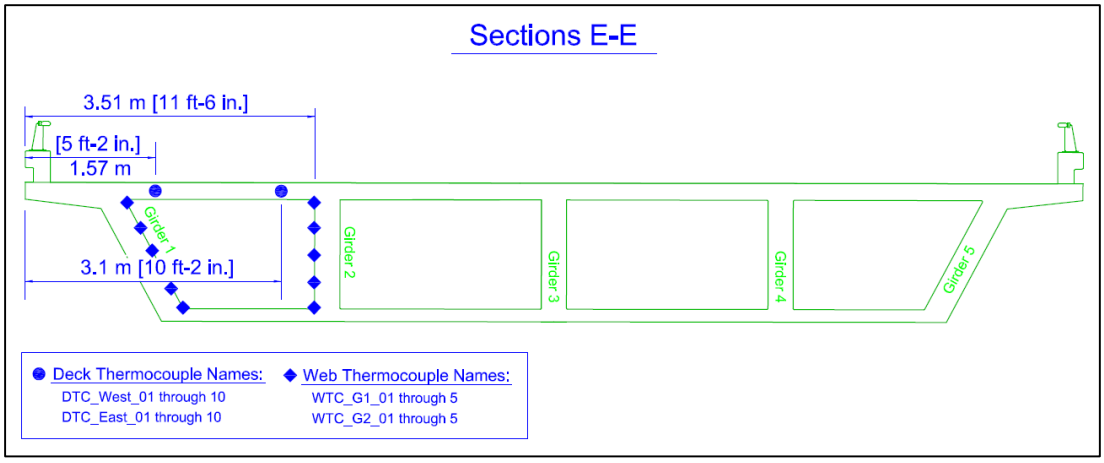

Figure 25: Sensor Locations at Section E-E

Figure 26 through Figure 31 show some of the installed sensors and data acquisition system for the SHM system. Figure 26 shows the installed system layout from below with protective boxes. Figure 27 shows a vibrating-wire strain gauge next to a Hitec strain gauge and Figure 28 shows an installed tiltmeter. Figure 29 shows an uninstalled velocity transducer and the deck thermocouples inside the pipe configuration that was inserted through the bridge deck. Figure 30 shows the thermocouples on the web or vertical girder. Figure 31 shows the data acquisition systems.

Table 2: Sensor Names, Descriptions, & Locations I

Section	Name	Description	Longitudinal Location (m)	Transverse Location (m)	Depth Location (mm)
AA	TM_NAWall_AA	Tilt Meter, Notth Abutment Wall	0.00	5.03	508
BB	VT_UD_BB	Velocity Transducer, Under Deck	11.80	5.03	152
	SG_G3_TF_BB	Strain Gauge, Girder 3, Top Flange	11.80	6.40	460
	TC_G3_TF_BB	Thermocouple, Girder 3, Top Flange	11.80	6.40	460
	SG_G3_BF_BB	Strain Gauge, Girder 3, Bottom Flange	11.80	6.40	1680
	TC_G3_BF_BB	Thermocouple, Girder 3, Bottom Flange	11.80	6.40	1680
CC	VT_UD_CC	Velocity Transducer, Under Deck	23.60	5.03	152
	SG_G1_BF_CC	Strain Gauge, Girder 1, Bottom Flange	23.60	1.75	1680
	TC_G1_BF_CC	Thermocouple, Girder 1, Bottom Flange	23.60	1.75	1680
	SG_G2_BF_CC	Strain Gauge, Girder 2, Bottom Flange	23.60	3.61	1680
	VWS_G2_BF_CC	Vibrating Wire, Girder 2, Bottom Flange	23.60	3.61	1680
	TC_G2_BF_CC	Thermocouple, Girder 2, Bottom Flange	23.60	3.61	1680
	SG_G3_TF_CC	Strain Gauge, Girder 3, Top Flange	23.60	6.35	457
	TC_G3_TF_CC	Thermocouple, Girder 3, Top Flange	23.60	6.35	457
	SG_G3_BF_CC	Strain Gauge, Girder 3, Bottom Flange	23.60	6.35	1680
	TC_G3_BF_CC	Thermocouple, Girder 3, Bottom Flange	23.60	6.35	1680
	SG_G4_BF_CC	Strain Gauge, Girder 4, Bottom Flange	23.60	9.09	1680
	VWS_G4_BF_CC	Vibrating Wire, Girder 4, Bottom Flange	23.60	9.09	1680
	SG_G5_BF_CC	Strain Gauge, Girder 5, Bottom Flange	23.60	10.95	1680
	TC_G5_BF_CC	Thermocouple, Girder 5, Bottom Flange	23.60	10.95	1680
DD	TM_Pier_DD	Tiltmeter, Central Pier	39.32	5.03	508
EE	DTC_WEST_01	Deck Thermocouple, West Device, 1	41.70	1.57	6.35
	DTC_WEST_02	Deck Thermocouple, West Device, 2	41.70	1.57	12.7
	DTC_WEST_03	Deck Thermocouple, West Device, 3	41.70	1.57	19.1
	DTC_WEST_04	Deck Thermocouple, West Device, 4	41.70	1.57	25.4
	DTC_WEST_05	Deck Thermocouple, West Device, 5	41.70	1.57	38.1
	DTC_WEST_06	Deck Thermocouple, West Device, 6	41.70	1.57	50.8
	DTC_WEST_07	Deck Thermocouple, West Device, 7	41.70	1.57	76.2
	DTC_WEST_08	Deck Thermocouple, West Device, 8	41.70	1.57	101.6
	DTC_WEST_09	Deck Thermocouple, West Device, 9	41.70	1.57	139.7
	DTC_WEST_10	Deck Thermocouple, West Device, 10	41.70	1.57	190.5
	WTC_G1_01	Web Thermocouple, Girder 1, 1	41.70	1.22	203.2
	WTC_G1_02	Web Thermocouple, Girder 1, 2	41.70	2.64	508.0
	WTC_G1_03	Web Thermocouple, Girder 1, 3	41.70	1.60	838.2
	WTC_G1_04	Web Thermocouple, Girder 1, 4	41.70	1.80	1168.4
	WTC_G1_05	Web Thermocouple, Girder 1, 5	41.70	1.98	1473.2
	DTC_EAST_01	Deck Thermocouple, East Device, 1	41.70	3.10	6.35
	DTC_EAST_02	Deck Thermocouple, East Device, 2	41.70	3.10	12.7
	DTC_EAST_03	Deck Thermocouple, East Device, 3	41.70	3.10	19.1
	DTC_EAST_04	Deck Thermocouple, East Device, 4	41.70	3.10	25.4
	DTC_EAST_05	Deck Thermocouple, East Device, 5	41.70	3.10	38.1
	DTC_EAST_06	Deck Thermocouple, East Device, 6	41.70	3.10	50.8
	DTC_EAST_07	Deck Thermocouple, East Device, 7	41.70	3.10	76.2
	DTC_EAST_08	Deck Thermocouple, East Device, 8	41.70	3.10	101.6
	DTC_EAST_09	Deck Thermocouple, East Device, 9	41.70	3.10	139.7
	DTC_EAST_10	Deck Thermocouple, East Device, 10	41.70	3.10	190.5
	WTC_G2_01	Web Thermocouple, Girder 2, 1	41.70	3.51	203.2
	WTC_G2_02	Web Thermocouple, Girder 2, 2	41.70	3.51	533.4
	WTC_G2_03	Web Thermocouple, Girder 2, 3	41.70	3.51	863.6
	WTC_G2_04	Web Thermocouple, Girder 2, 4	41.70	3.51	1193.8
	WTC_G2_05	Web Thermocouple, Girder 2, 5	41.70	3.51	1498.6

Section	Name	Description	Longitudinal Location (m)	Transverse Location (m)	Depth Location (mm)
FF	VT_UD_FF	Velocity Transducer, Under Deck	51.10	5.03	152
	SG_G3_TF_FF	Strain Gauge, Girder 3, Top Flange	51.10	6.40	460
	TC_G3_TF_FF	Thermocouple, Girder 3, Top Flange	51.10	6.40	460
	SG_G3_BF_FF	Strain Gauge, Girder 3, Bottom Flange	51.10	6.40	1680
	TC_G3_BF_FF	Thermocouple, Girder 3, Bottom Flange	51.10	6.40	1680
GG	VT_UD_GG	Velocity Transducer, Under Deck	62.91	5.03	152
	SG_G1_BF_GG	Strain Gauge, Girder 1, Bottom Flange	62.91	1.75	1680
	TC_G1_BF_GG	Thermocouple, Girder 1, Bottom Flange	62.91	1.75	1680
	SG_G2_BF_GG	Strain Gauge, Girder 2, Bottom Flange	62.91	3.61	1680
	VWS_G2_BF_GG	Vibrating Wire, Girder 2, Bottom Flange	62.91	3.61	1680
	TC_G2_BF_GG	Thermocouple, Girder 2, Bottom Flange	62.91	3.61	1680
	SG_G3_TF_GG	Strain Gauge, Girder 3, Top Flange	62.91	6.35	457
	TC_G3_TF_GG	Thermocouple, Girder 3, Top Flange	62.91	6.35	457
	SG_G3_BF_GG	Strain Gauge, Girder 3, Bottom Flange	62.91	6.35	1680
	TC_G3_BF_GG	Thermocouple, Girder 3, Bottom Flange	62.91	6.35	1680
	SG_G4_BF_GG	Strain Gauge, Girder 4, Bottom Flange	62.91	9.09	1680
	VWS_G4_BF_GG	Vibrating Wire, Girder 4, Bottom Flange	62.91	9.09	1680
	SG_G5_BF_GG	Strain Gauge, Girder 5, Bottom Flange	62.91	10.95	1680
	TC_G5_BF_GG	Thermocouple, Girder 5, Bottom Flange	62.91	10.95	1680
HH	TM_SAWall_HH	Tiltmeter South, Abutment Wall	78.64	5.03	508

Figure 26: System Layout from Below

Figure 27: Vibrating Wire & Hitec Strain Gauges

Figure 28: Tiltmeter

Figure 29: Uninstalled Velocity Transducer & Deck Thermocouples

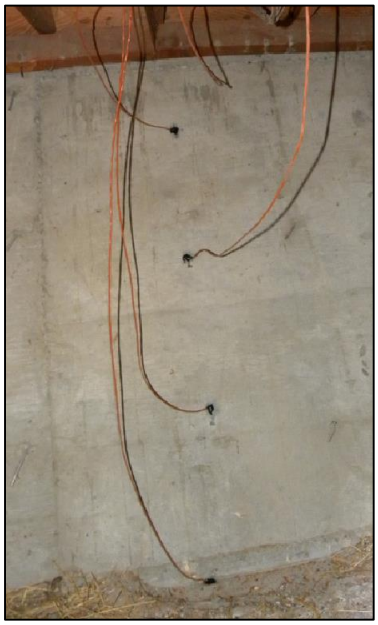

Figure 30: Web Thermocouples

Once the SHM system was installed, the data acquisition was programmed to measure the slow sampling rate records every 15 minutes, as explained before.

Figure 31: Data Acquisition Systems

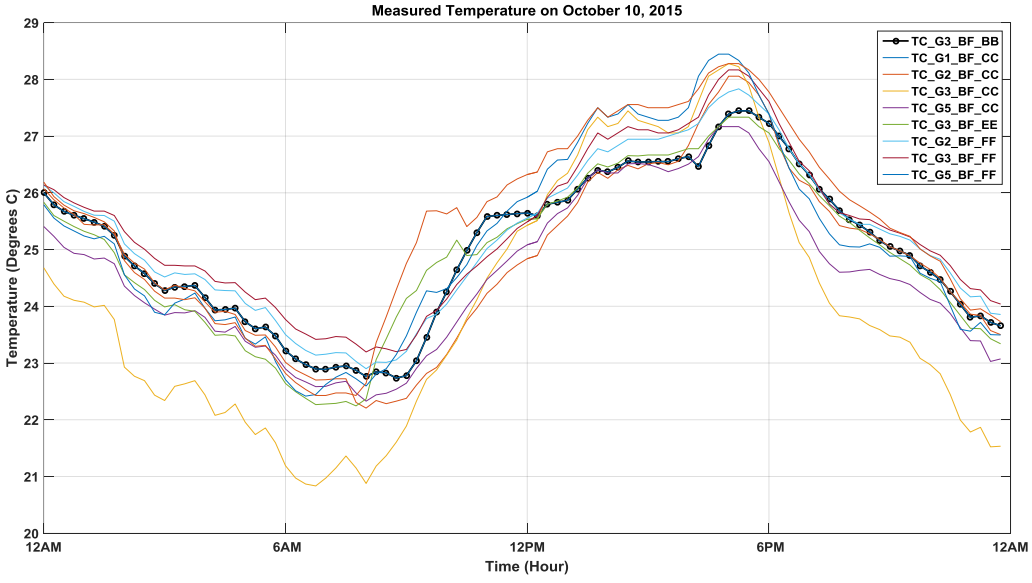

Figure 32: Daily Temperature Measurements (October 10, 2015)

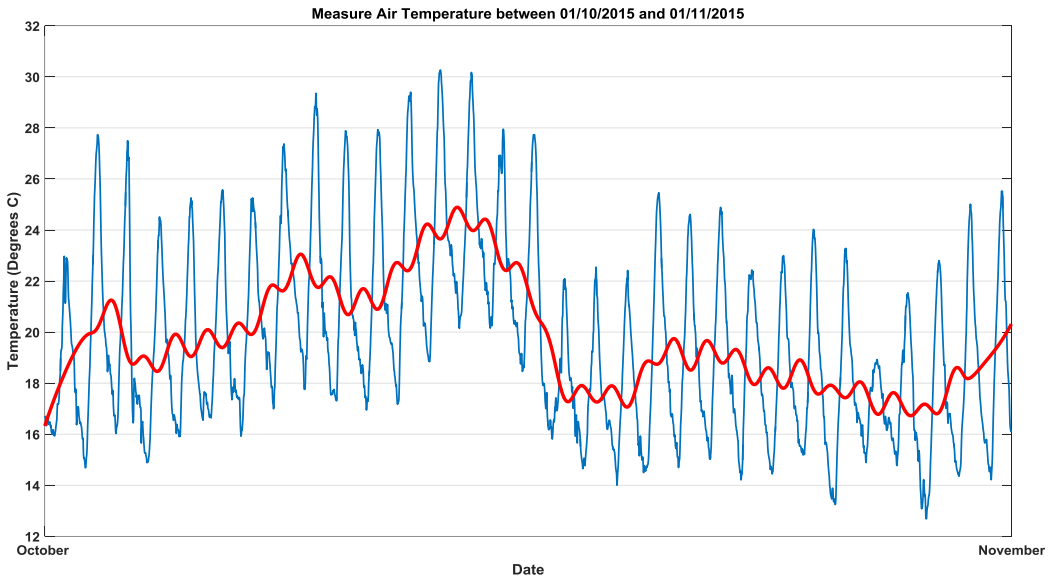

Figure 33: California Bridge Temperature Trend

Salt Lake Bridge

The Salt Lake Bridge is an overpass bridge on the 21st South Interchange of I-15 in Salt Lake City, Utah. The bridge serves as a connector from westbound I-80 to westbound SR-201. The bridge includes four individual structures containing a total of 25-spans with a total length of 1.14 km (3741 feet). The instrumentation and modeling was confined to a single 13-span structure with two expansion joints shown in Figure 34.

Salt Lake Bridge is a 13-span 722.65-meter long reverse curve steel girder bridge constructed during the I-15 Interstate corridor reconstruction project and was completed in 2000.

The spans are constructed of a transversely post-tensioned concrete deck supported by three steel girders. Reinforcing steel is epoxy-coated M284. Structural steel is ASHTO M270M Grade 345. The strength of the cast-in-place concrete is f'_c = 28 MPa (4060 psi) with a 5 percent

silica fume content (by weight). The steel girders are continuous, bearing on concrete-filled steel pipe piles. The bearing soils consist of extremely deep sofeet sediments.

The structure serves the purpose of connecting commuters traveling westbound from I-80 to the State of Utah's State Road 201 (SR-201), by crossing over I-15. Located among a number of other freeway interchanges, the structure traverses over the top of all but one providing a structure built on very tall columns. Of these columns, the minimum height is 12.61 meters and the maximum height is 23.80 meters, measured from the top of their respective foundations to the bottom of the bent cap.

Several structures in the 21st South Interchange were considered. It was decided to choose a structure with the number one priority to be placed on its research significance. The location of the selected bridge proved to be very difficult to access and instrument, but the selected bridge did provide the desired characteristics. The structure only carries traffic on two lanes in one direction, and is therefore a rather narrow structure with an outside deck width of 12.92 meters. The width, height and length characteristics, combined with the relatively light mass of the structure, result in a structure that is well suited for dynamic testing. The instrumentation was limited to the center portion of structure as can be seen in Figure 35.

Temperature data were collected from a weather station in south of Salt Lake City. Figure 356 shows the trend of temperature from November 1, 2014 to May 1, 2015.

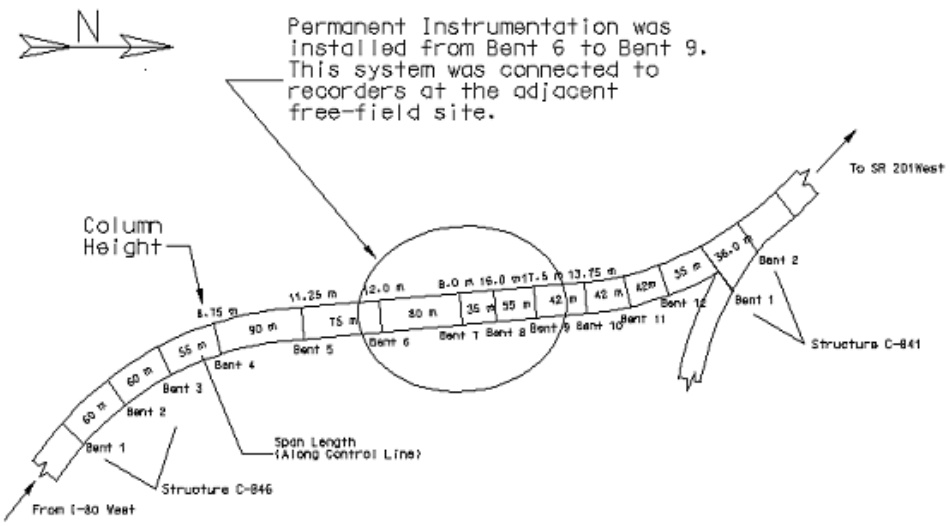

Figure 34: Instrumentation of Salt Lake Bridge (Halling, 2006)

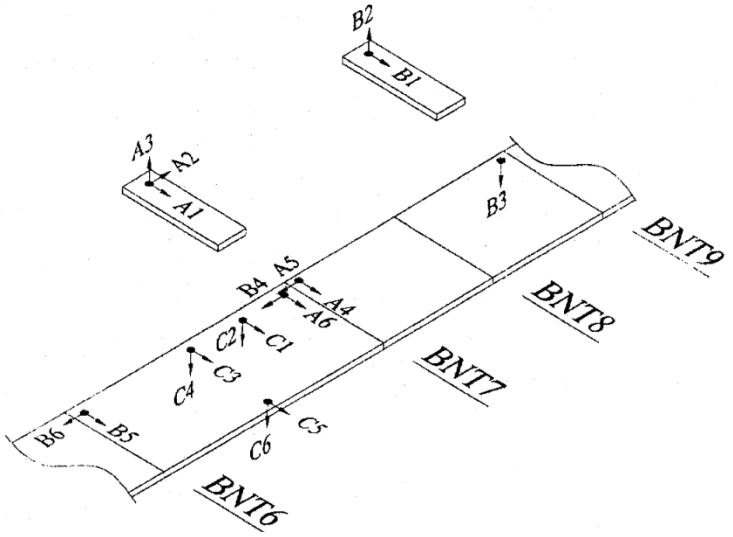

Figure 35: Sensors Layout

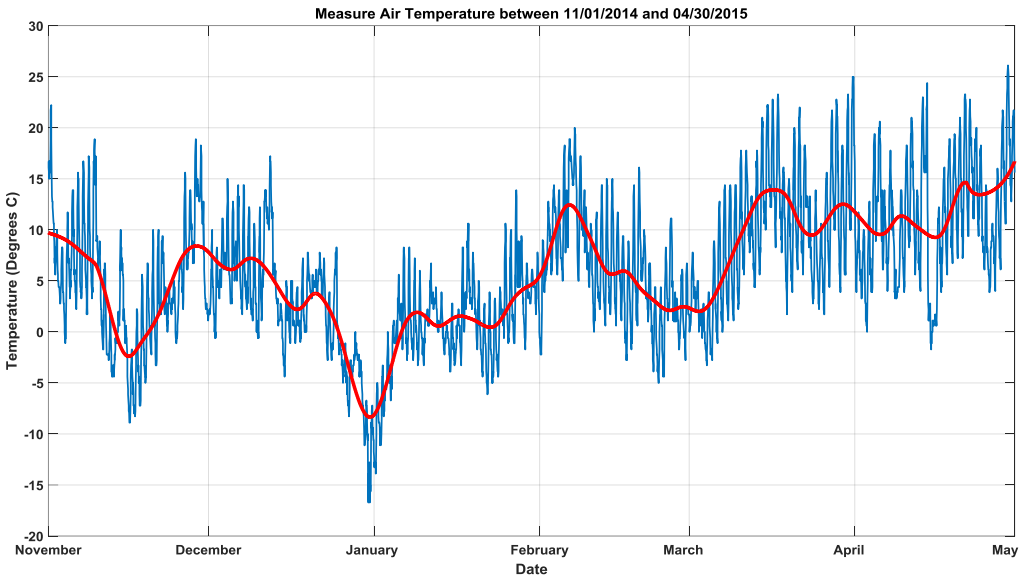

Figure 36: Salt Lake Bridge Temperature Trend

		November 2014	December 2014	January 2015	February 2015	March 2015	April 2015
Air Temperature (Degrees C)	Mean	4.76	2.39	1.15	6.36	10.57	11.68
	STD	6.19	5.99	3.96	5.34	6.12	5.90

Chapter 4: System Identification and Dynamic Properties

Modal identification techniques are divided to two main categories, input-output and output-only. Input-output are referred to techniques when both loads (input) and structure responses (output) are measured and available for modal identification. However, civil engineering structures, such as bridges, are usually monitored by collecting vibration response while measuring the input excitation is not simply possible. In these cases, output-only methods are used for identifying the modal parameters.

The classical approach is to use a discrete Fourier transform (DFEET) and based on the peaks, well separated natural frequencies and mode shapes can be estimated. This method is fast and simple to use and gives some insights to the researchers of how the structure actually behaves. However, close modes may not be detected simply. The frequency resolution is an important factor in frequency estimation and estimated damping ratios are very uncertain.

Frequency Domain Decomposition (FDD)

This method is an extension of the peak picking method. Modal parameters are estimated through singular value decomposition (SVD) of the spectral matrix.

$$G_{yy}(jw) = \bar{H}(jw)G_{xx}(jw)H^T(jw)$$

When the loading is white noise and the structure is lightly damped, the result is exact.

Taking the singular value decomposition (SVD) of the spectral matrix

$$G_{yy}(jw) = U_i S_i {U_i}^H$$

U_i is a unitary matrix holding the singular vectors U_{ij}, S_i is a diagonal matrix holding the scalar singular values S_{ij}.

The SVD decomposed the spectral matrix into single degree of freedom functions. When the structure is lightly damped, the contribution of different modal modes at a particular frequency is limited to one or two and provided singular values can be associated with the natural frequencies of the tested structure.

This method was used to initially estimate the natural frequencies of the studied structure for further analysis with Eigen system Realization Algorithm.

Lab Specimen

To identify the natural frequency of the lab specimen acceleration records were used. The spectrum matrix elements were calculated with the Welch method using time segments of 4096 points, a Hanning window and 50 percent overlap. A few impact loads were applied to the beam for each dynamic test performed every hour. Figure 37 shows a typical recorded acceleration data measured through BDI system.

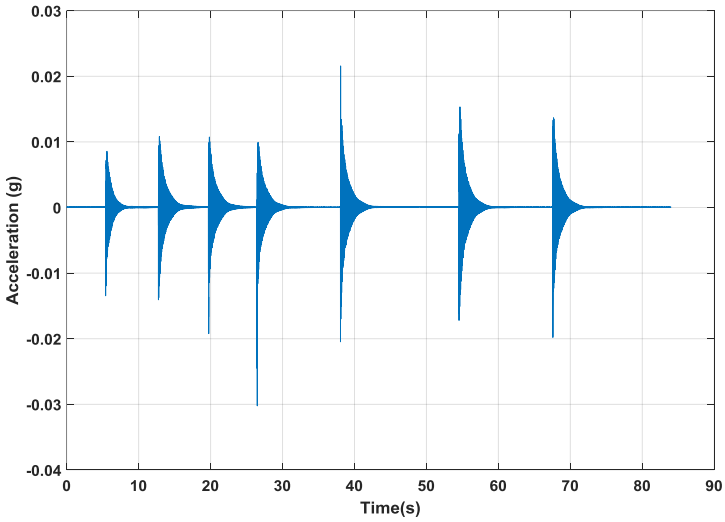

Figure 37: Typical Recorded Acceleration

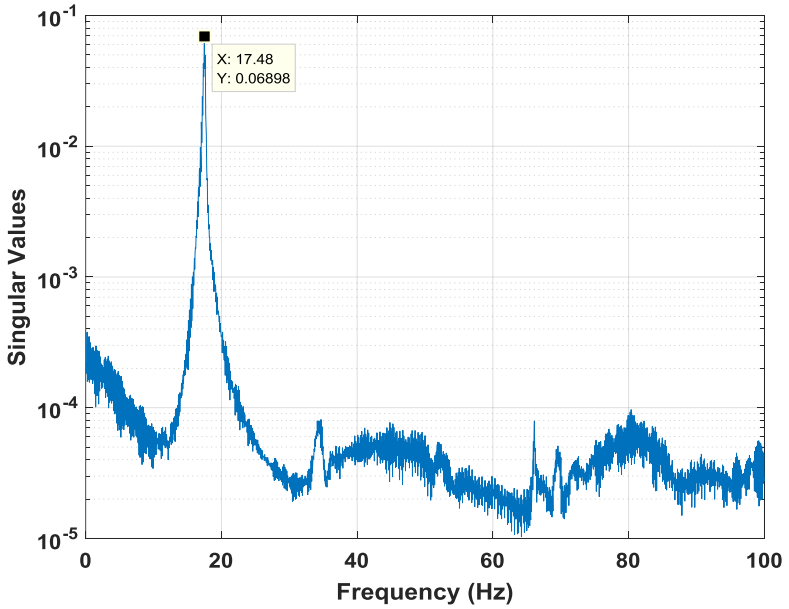

Figure 38: Estimation of the Natural Frequencies with FDD Method

The boundary conditions for the lab specimen are considered as pinned-roller. Therefore, the frequencies of this beam can be calculated by the following equation

$$f = \frac{n^2 \pi}{2L^2} \sqrt{\frac{EI}{\rho}}$$

Equation 1

where

n is the mode number

E is the modulus of elasticity (2e+11 pa)

I is the area moment of intertia (4.162e-7 m^4)

L is the length of the beam (1.829m)

ρ is mass density (60.387 kg/m)

Theoretical calculated natural frequency of the specimen was used to validate the estimated natural frequency of the specimen from measured acceleration response (Table 3).

Table 3: Initial Identified Natural Frequency

	Theoretical Frequency (Hz)	Identified Frequency (Hz)
Mode 1	17.44	17.48

Perry Bridge

Dynamic responses of Perry Bridge to ambient excitations are recorded every hour for 3 minutes. While the sampling frequency of the data acquisition recorder was set to 100 Hz each set of data had (3*60*100=18000) samples (Figure 39). Figure 42 shows the initial estimation of Perry Bridge natural frequencies with FDD method.

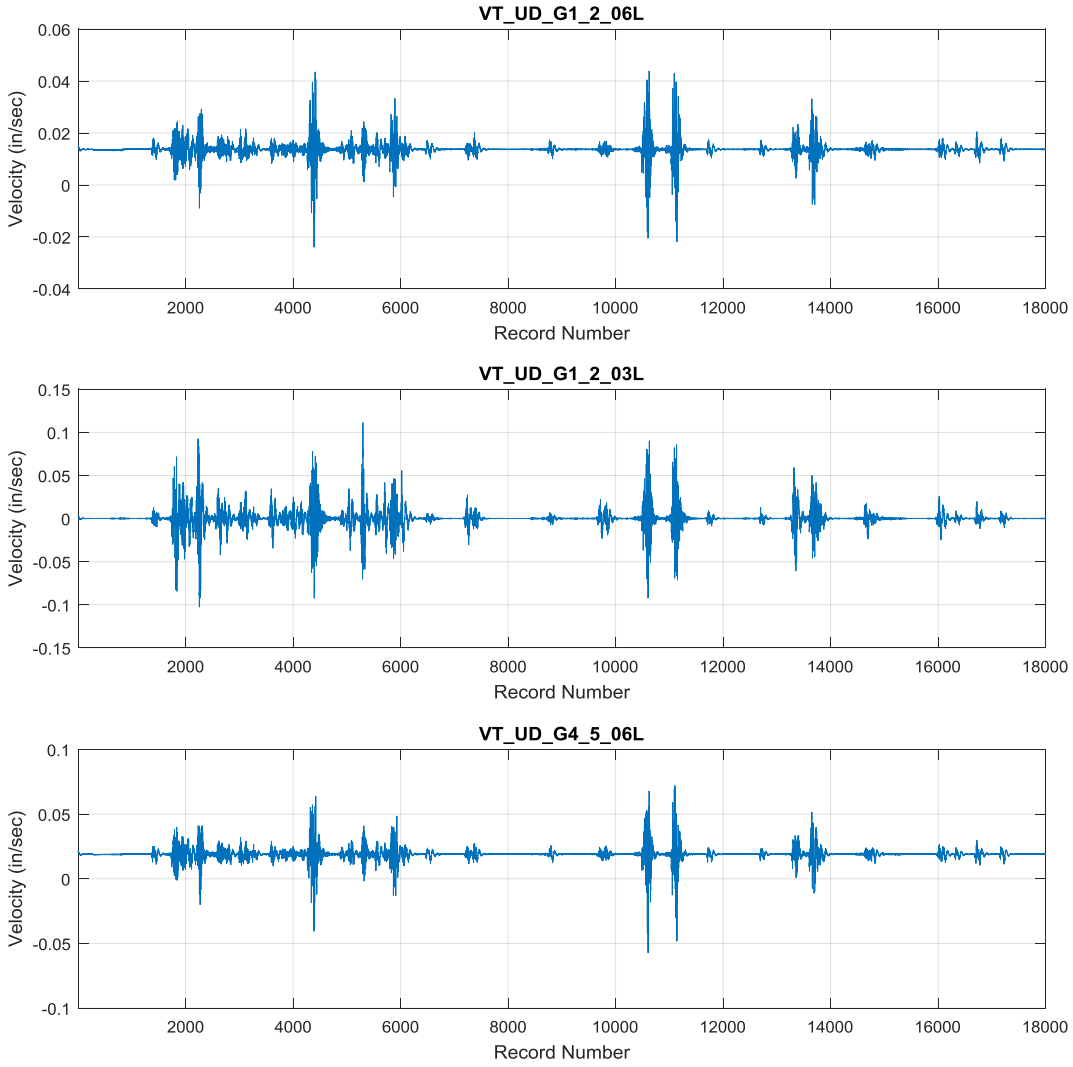

Figure 39: Typical Velocity Measurements from Perry Bridge

The spectrum matrix elements were calculated with the Welch method using time segments of 4096 points, a Hanning window and 50 percent overlap.

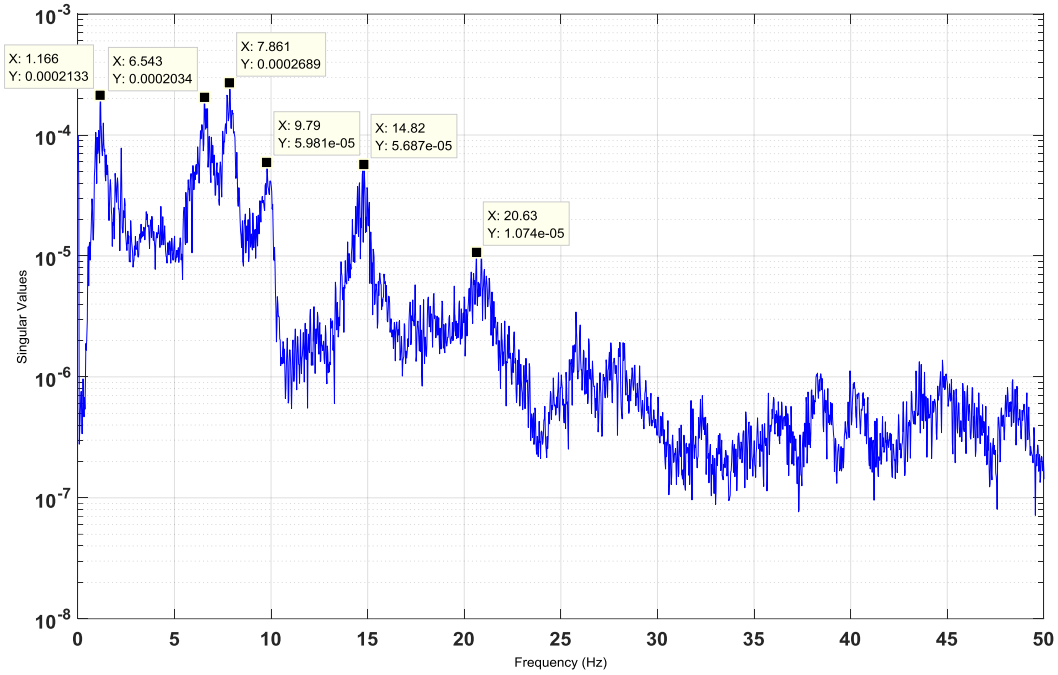

Figure 40: Estimation of the Perry Bridge Natural Frequencies with FDD Method

The initial estimation of Perry Bridge natural frequencies is presented in Table 4.

Table 4: Initial Identified Natural Frequencies

	Identified Frequency (Hz)
Mode 1	1.17
Mode 2	6.54
Mode 3	7.86
Mode 4	9.79
Mode 5	14.82
Mode 6	20.63

California Bridge

Dynamic responses of California Bridge to ambient excitations are recorded every hour for 6 minutes. While the sampling frequency of the data acquisition recorder was set to 50 Hz each set of data had (6*60*50=18000) samples (Figure 41). Figure 42 shows the initial estimation of California Bridge natural frequencies with FDD method.

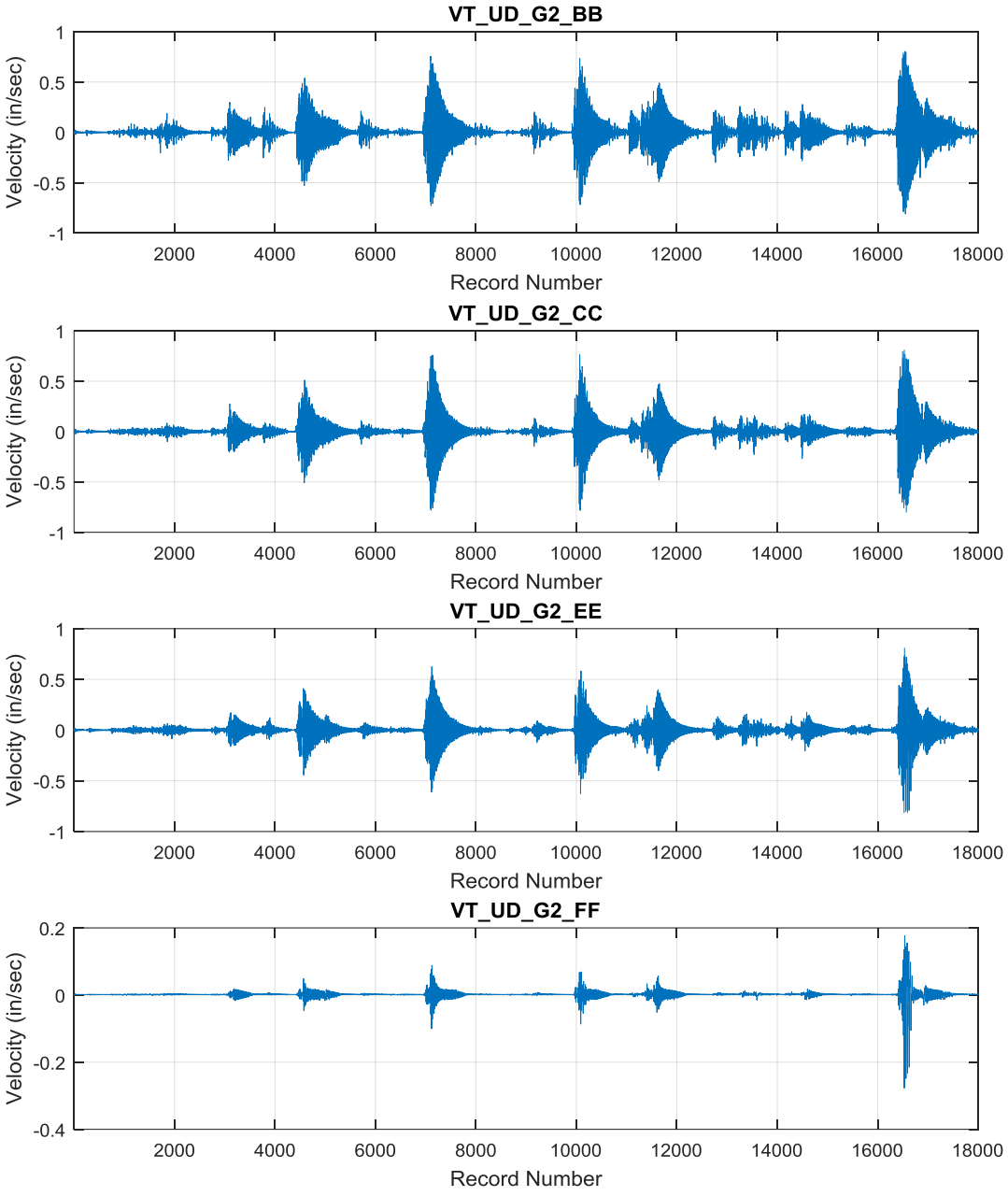

Figure 41: Typical Velocity Measurements from California Bridge

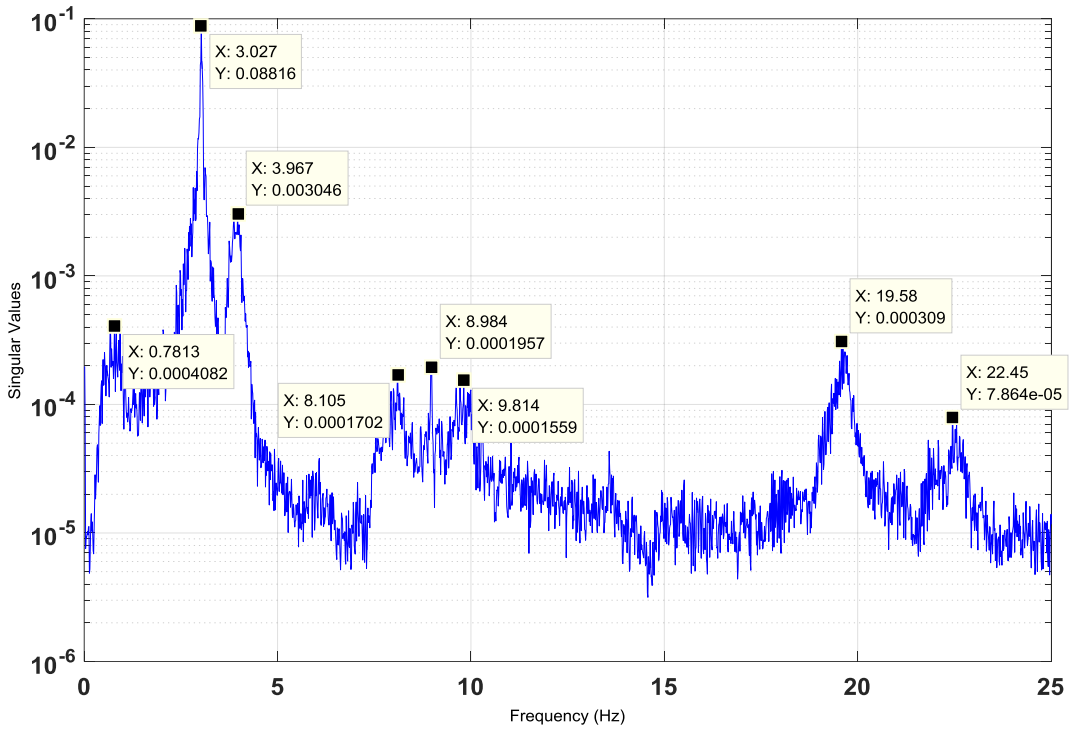

Figure 42: Estimation of the California Bridge Natural Frequencies with FDD Method

The initial estimation of California Bridge natural frequencies are presented in Table 4.

Table 5: Initial Identified Natural Frequencies

	Identified Frequency (Hz)
Mode 1	0.78
Mode 2	3.03
Mode 3	3.97
Mode 4	8.10
Mode 5	8.98
Mode 6	9.81
Mode 7	19.58
Mode 8	22.45

Salt Lake Bridge

Dynamic responses of Salt Lake Bridge to ambient excitations are recorded every hour for 3 minutes. While the sampling frequency of the data acquisition recorder was set to 100 Hz each set of data had (3*60*100=18000) samples (Figure 43). Figure 42 shows the initial estimation of Salt Lake Bridge natural frequencies with FDD method.

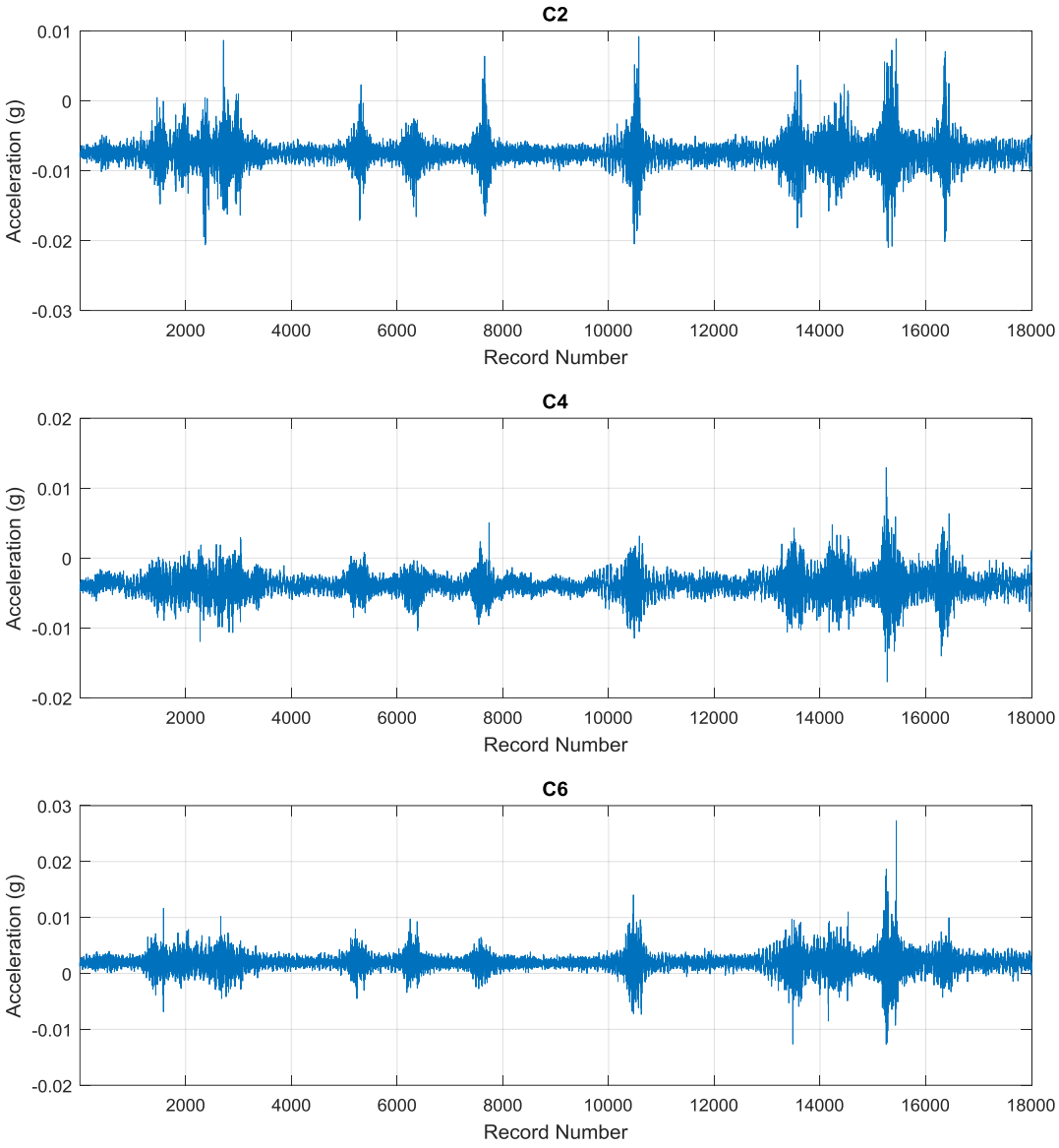

Figure 43: Typical Acceleration Measurements from Salt Lake Bridge

The initial estimation of California Bridge natural frequencies are presented in Table 4.

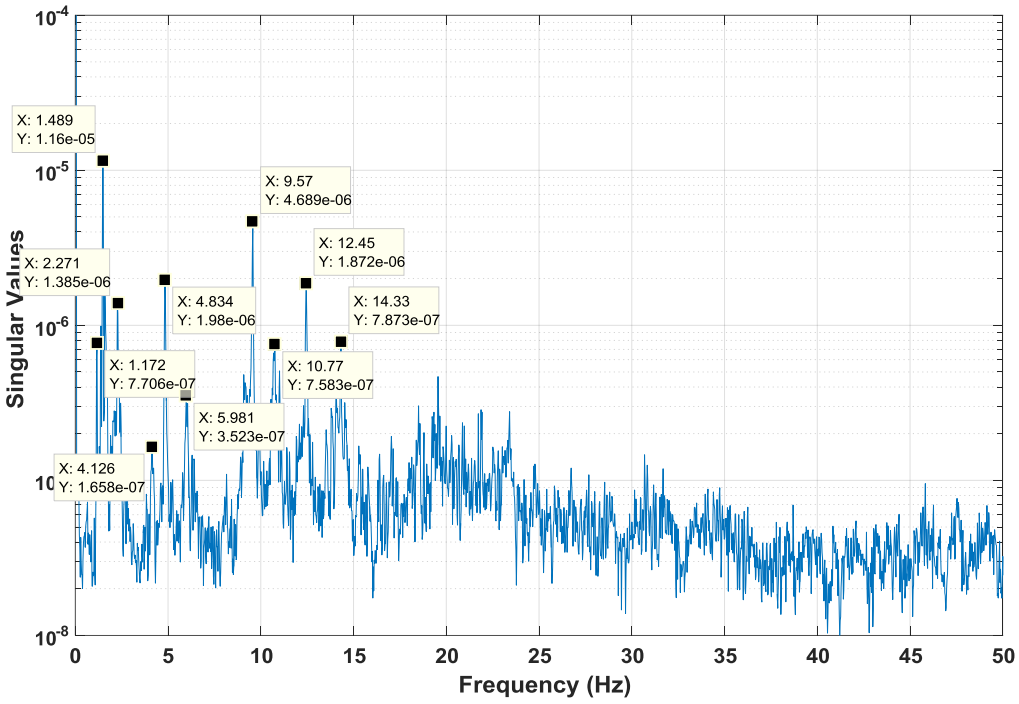

Figure 44: Estimation of the Natural Frequencies with FDD Method

Table 6: Initial Identified Natural Frequencies

	Identified Frequency (Hz) Mean
Mode 1	1.17
Mode 2	1.49
Mode 3	2.27
Mode 4	4.13
Mode 5	4.83
Mode 6	5.98
Mode 7	9.57
Mode 8	10.77
Mode 9	12.45
Mode 10	14.33

Eigensystem Realization Algorithm (ERA)

Output-only system identification offered numerical techniques to extract modal parameters from measured outputs while input excitation is unknown. These methods were used for modal identification of this structure since there is no information available on the excitation applied to the system.

Eigensystem Realization Algorithm (ERA) is one of the very common system identification techniques that have been used for modal identification of different structures (Caicedo 2011). This method was first developed based on free response measurements from impulse excitations. If the free response of the structure is not directly available, there are a few estimation techniques that can provide an estimation of free response. Natural Excitation Technique (NExT) is one of the techniques that enables the use of the ERA with ambient vibration (James III et al. 1993). This technique was first developed for the modal testing of a wind turbine. It was shown in that study that the cross-correlation function of two responses due

to a white noise input has the characteristics as the impulse response function of the original system. In this study, cross-spectral density function and taking its inverse Fourier transform was used to estimate the correlation functions. The number of points for the FFEET was set to 2048 and the number of data points overlapping between data blocks was set to 1024 i.e. 50 percent overlap. Then, ERA provides a numerical technique to compute the state-space model from an estimate of the impulse responses. A linear-time invariant system can be represented with following state-space equations in discrete time

$$x(k+1) = Ax(k) + Bu(k)$$

$$y(k) = Cx(k) + Du(k)$$

$x(k)$ is the state vector, *u* is the input vector and *y* is the system outputs. A, B, C and D are state-space matrices. Since the input to the system is unknown when ERA is used with NExT here, matrices B and D cannot be computed. The system realization begins by forming the Hankel matrix.

$$H(k) = \begin{bmatrix} Y(k+1) & Y(k+2) & \cdots & Y(k+m) \\ Y(k+2) & Y(k+3) & & Y(k+m+1) \\ \vdots & & \ddots & \vdots \\ Y(k+n) & Y(k+n+1) & \cdots & Y(k+m+n) \end{bmatrix}$$

The next step is the factorization of the *H(0)* by use of singular value decomposition (SVD).

$$SVD\ [H(0)] = R\Sigma S^T$$

The columns of matrices R and S are orthonormal and Σ is a rectangular matrix.

$$\Sigma = \begin{bmatrix} \Sigma_n & 0 \\ 0 & 0 \end{bmatrix}$$

Σ_n is an n by n matrix and n is the number of poles. In real applications, the diagonal terms of Σ are not exactly zero and the smaller singular values will be eliminated to obtain a minimum realization of the system. One solution for the state matrix A and C is based on the following equations:

$$A = {\Sigma_n}^{-1/2} R^T H(1) S_n {\Sigma_n}^{-1/2}$$

$$C = the\ first\ m\ rows\ of\ R_n {\Sigma_n}^{-1/2}$$

Lab Specimen

The results of system identification of the lab specimen with NExT-ERA for the 11 data samples in 11 hours are shown in Figure 45.

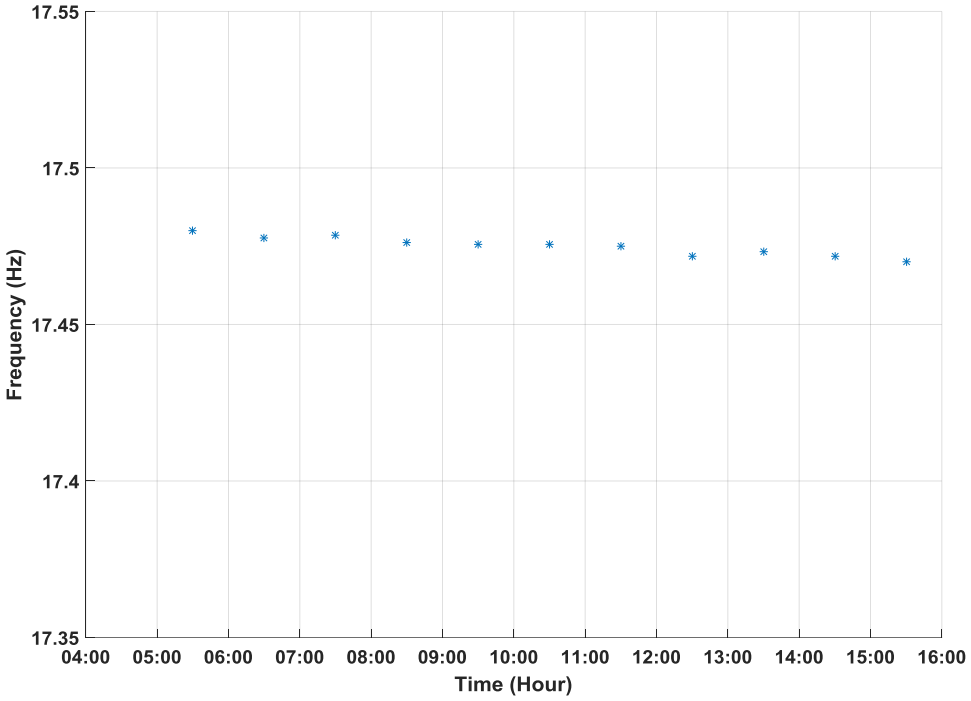

Figure 45: Variation of the Natural Frequencies of the Lab Specimen in 11 Hours

Perry Bridge

The results of system identification of Perry Bridge with NExT-ERA between January 1 and July 1, 2015 are shown in Figure 45.

Figure 46: Variation of the Natural Frequencies of the Five Modes between January 1 and July 1, 2015

Table 7: Identified Natural Frequencies in the Period of 6 Months

	Identified Frequency (Hz) Mean	Identified Frequency (Hz) Standard Deviation
Mode 1	6.38	0.63
Mode 2	8.28	0.91
Mode 3	9.80	0.83
Mode 4	13.89	1.36
Mode 5	19.07	1. 42

California Bridge

The results of system identification of California Bridge with NExT-ERA between October 1 and November 1, 2015 are shown in Figure 47.

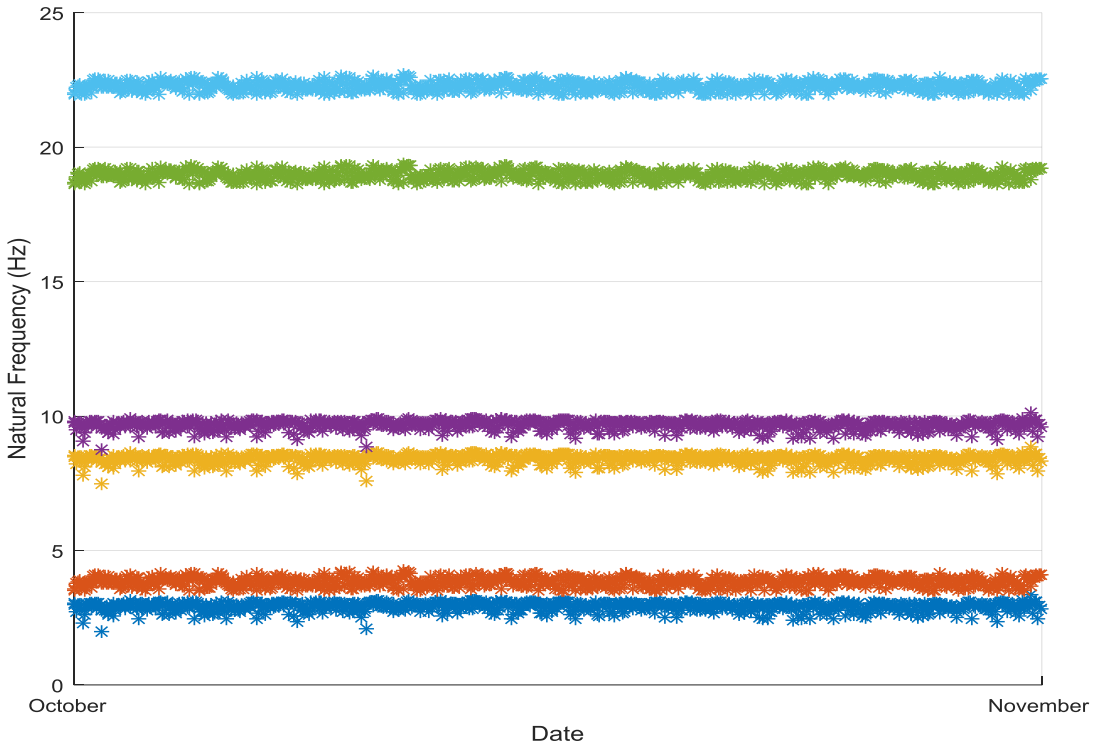

Figure 47: Variation of the Natural Frequencies of the Six Modes Between October 1 and November 1, 2015

Table 8: Identified Natural Frequencies in the Period of 1 Month

	Identified Frequency (Hz) Mean	Identified Frequency (Hz) Standard Deviation
Mode 1	2.91	0.17
Mode 2	3.83	0.17
Mode 3	8.52	1.14
Mode 4	9.84	0.32
Mode 5	19.68	0.84
Mode 6	22.51	0.96

Salt Lake Bridge

The results of system identification of Salt Lake Bridge with NExT-ERA between November 1, 2014 and May 1, 2015 are shown in Figure 48.

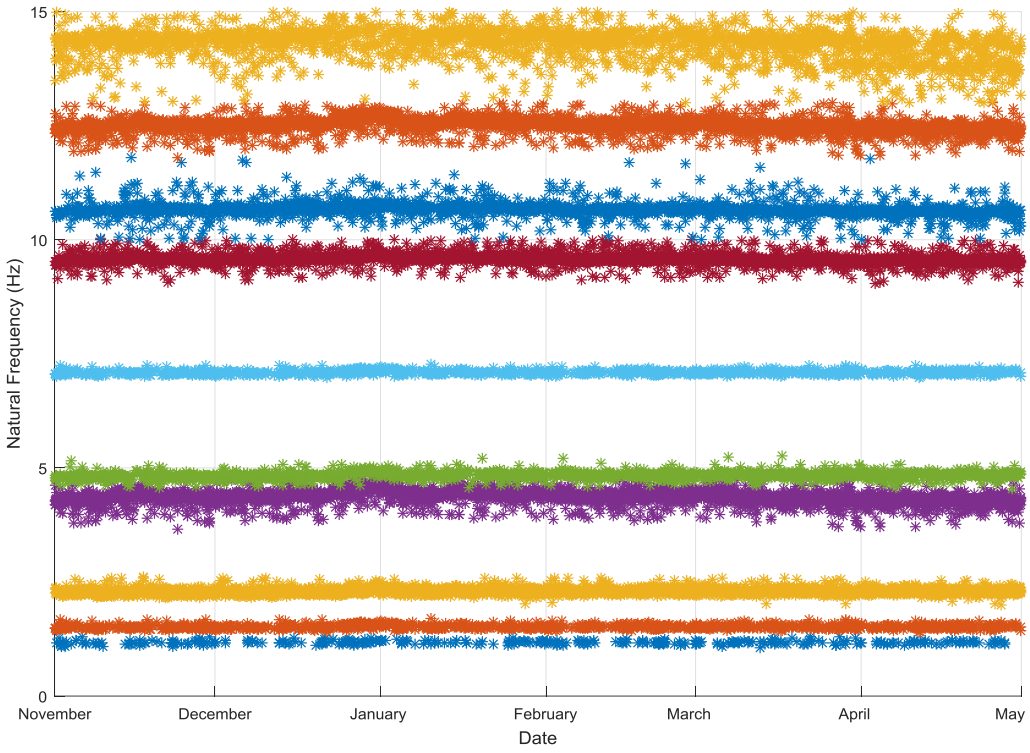

Figure 48: Variation of the Natural Frequencies of the Ten Modes Between November 1, 2014 and May 1, 2015

Table 9: Identified Natural Frequencies in the Period of 6 Months

	Identified Frequency (Hz) Mean	Identified Frequency (Hz) Standard Deviation
Mode 1	1.18	0.04
Mode 2	1.52	0.04
Mode 3	2.30	0.06
Mode 4	4.12	0.33
Mode 5	4.83	0.08
Mode 6	6.14	0.39
Mode 7	9.58	0.11
Mode 8	10.66	0.18
Mode 9	12.50	0.15
Mode 10	14.26	0.35

Chapter 5: Statistical Models

Linear Regression

In the linear polynomial model, natural frequencies of the structures assumed to be a linear combination of the measured temperatures.

$$\boldsymbol{Y = X\beta + e}$$

Equation 2

In this equation, Y is the measured frequencies with N (number of data points) rows and N_{mode} (number of identified frequencies) columns.

X is represents temperature measurements with N (number of data points) rows and N_T (number of temperature inputs) columns.

β matrix is the matrix of model coefficients with N_T (number of temperature inputs) rows and N_{mode} (number of identified frequencies) columns.

e is the matrix of errors with the same size as Y.

Linear ARX Model

Autoregressive models with exogenous inputs (ARX) have shown good results for modeling of natural frequencies vs. temperature (Sohn et al. 1999). These models have the form:

$$\boldsymbol{y(k) + a_1 y(k-1) + \cdots + a_{na} y(k-na)}$$
$$\boldsymbol{= b_1 u(k) + b_2 u(k-1) + \cdots + b_{nb} u(k-nk-nb-1) + e(k)}$$

Equation 3

where $y(k)$,$u(k)$ and $e(k)$ are the system output, input and noise respectively; na and nb are the maximum lags for the system output and input.

Nonlinear ARX (NARX) Model

This model was developed in 1981 to represent a wide class of nonlinear systems

$$\boldsymbol{y(k) = F[y(k-1), y(k-2), y(k-3) \ldots y(k-ny), u(k-d), u(k-d-1), \ldots u(k-d-nu), e(k-1), e(k-2), \ldots, e(k-ne)]}$$

Equation 4

where $y(k)$, $u(k)$ and $e(k)$ are the system output, input and noise sequences respectively; na and nb and ne are the maximum lags for the system output and input and noise. F[.] is some nonlinear function. NARX can model more complex input-output relationship (Billings 2013). The total number of potential model terms in a NARX model with *l* degree of nonlinearity is

$$\boldsymbol{M = (ny + nu + l)! \Big/ [(ny + nu)!\, l!]}$$

Equation 5

Different classes of models are available with Matlab function "nlarx". In this study, "wavenet" was used since it provided the best results. In this study, 60 percent of the data sets were randomly selected and used for training the model, 20 percent were used as cross validation test to avoid overfitting and 20 percent were used as test sets.

To quantify the goodness of fit between the data of these two models, the coefficient of determination (R^2) was used. The R^2 of the two models were compared in Table 10 through

Table 12. The results were improved by using the nonlinear models, but the cost of computation associated with calculation of model terms was significantly higher.

Lab Specimen

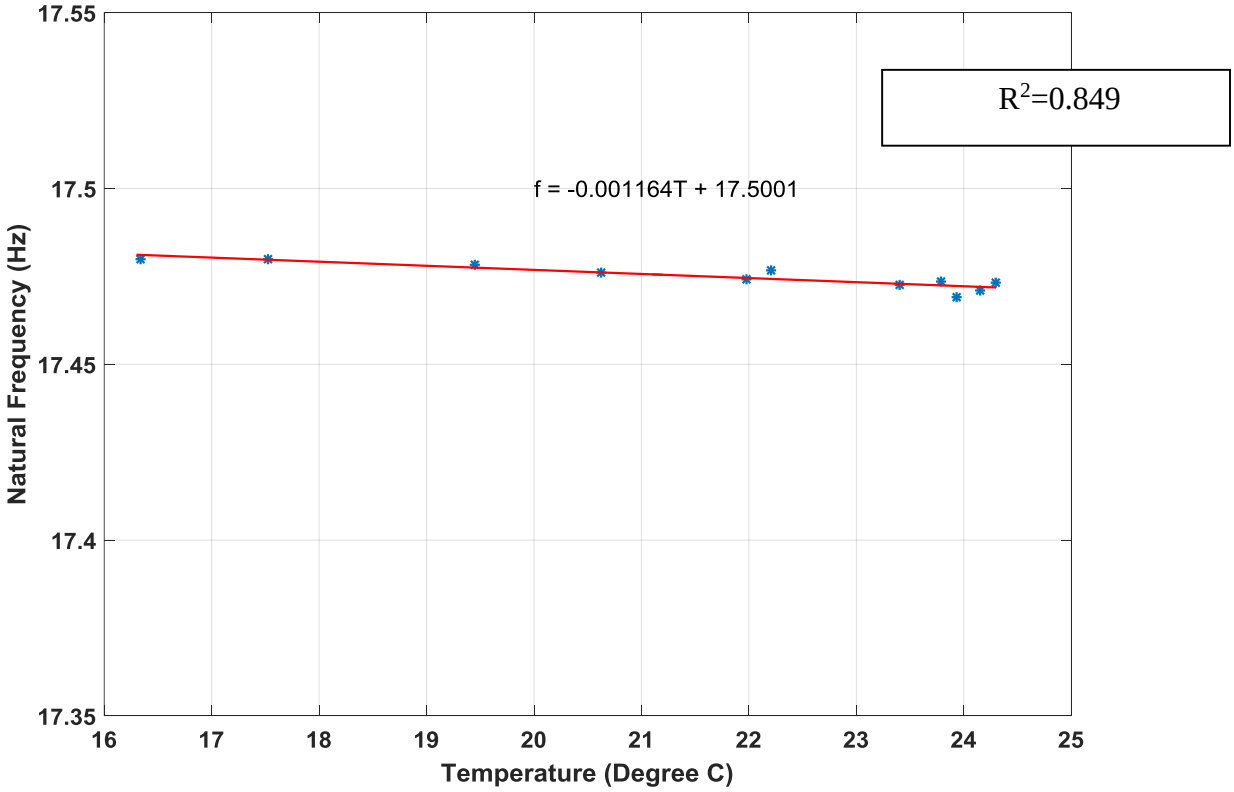

Figure 49: Relation of Natural Frequencies to Temperature of the Lab Specimen

Perry Bridge: Input Variable Selection

The number of temperature measurements on Perry Bridge was six including five temperature measurements on five girders of the bridge and the ambient temperature. The number of measurements useful for modeling can be estimated using principal component analysis. The singular value decomposition of the matrix formed by all temperature measurements can be utilized to provide a transformed set of variables. In these variables all

columns are mutually orthogonal. The number of relatively large singular values controls the number of independent measurements. In this case, 3 temperature measurements were used as inputs.

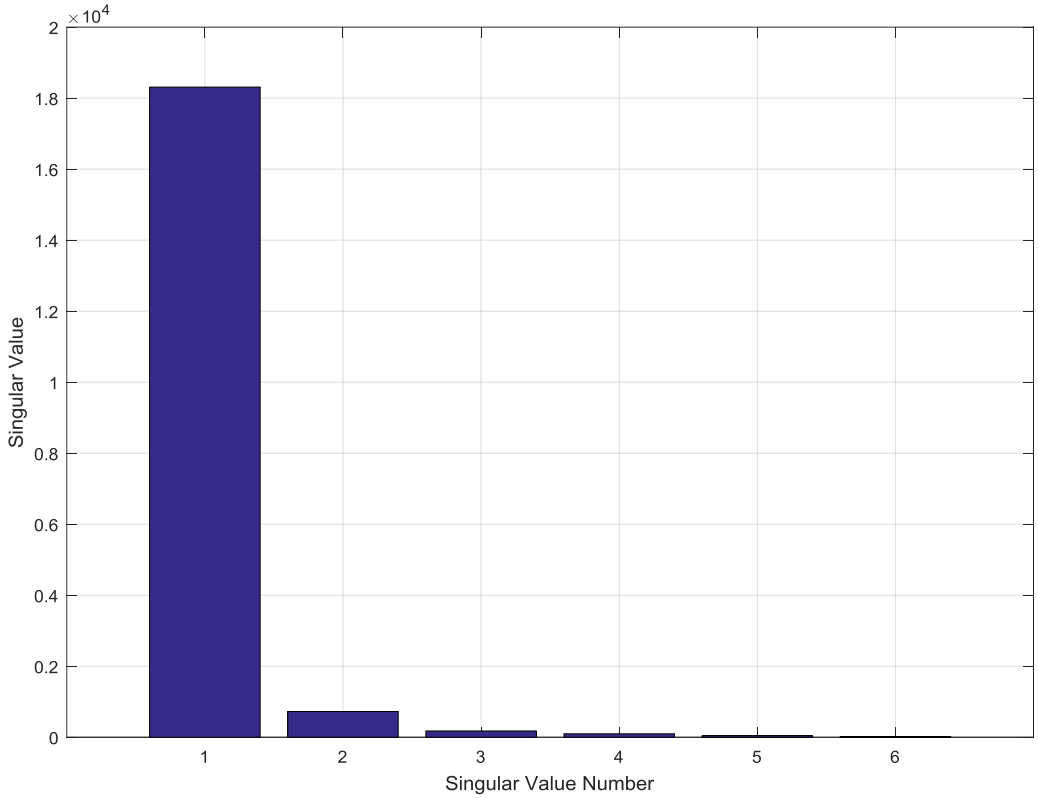

Figure 50: Singular Values from Principal Component Analysis of Temp. Measurements

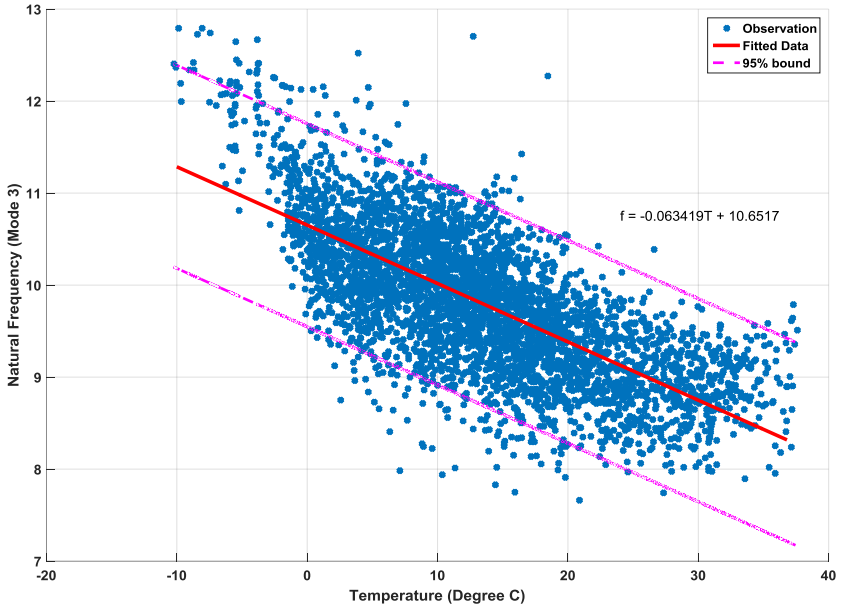

Figure 51: Relation of Natural Frequencies (3rd mode) to Temp. of the Perry Bridge

Table 10: Comparison of the Goodness of Fit (R2) for Linear, ARX and NARX Models

	Mode 1			Mode 2			Mode 3			Mode 4			Mode 5		
	Linear	ARX	NARX	Linear	ARX	NARX	Linear	ARX	NARX	Linear	ARX	NARX	Linear	ARX	NARX
Jan	0.421	0.639	0.700	0.464	0.711	0.756	0.467	0.719	0.724	0.502	0.729	0.772	0.441	0.513	0.692
Feb	0.489	0.713	0.779	0.478	0.736	0.746	0.397	0.747	0.804	0.471	0.749	0.777	0.490	0.526	0.597
Mar	0.429	0.719	0.720	0.452	0.713	0.741	0.420	0.716	0.747	0.480	0.723	0.814	0.465	0.524	0.600
Apr	0.509	0.723	0.729	0.478	0.704	0.706	0.426	0.754	0.765	0.405	0.759	0.760	0.468	0.530	0.606
May	0.510	0.680	0.740	0.464	0.639	0.669	0.476	0.691	0.739	0.432	0.684	0.687	0.503	0.499	0.583
June	0.454	0.700	0.736	0.403	0.616	0.626	0.434	0.693	0.779	0.508	0.710	0.716	0.484	0.537	0.609

California Bridge: Input Variable Selection

The number of temperature measurements on California Bridge was 51 while five of the sensors were not functional. The same method that was previously used for Perry Bridge provided the best number of inputs. In this case it is four.

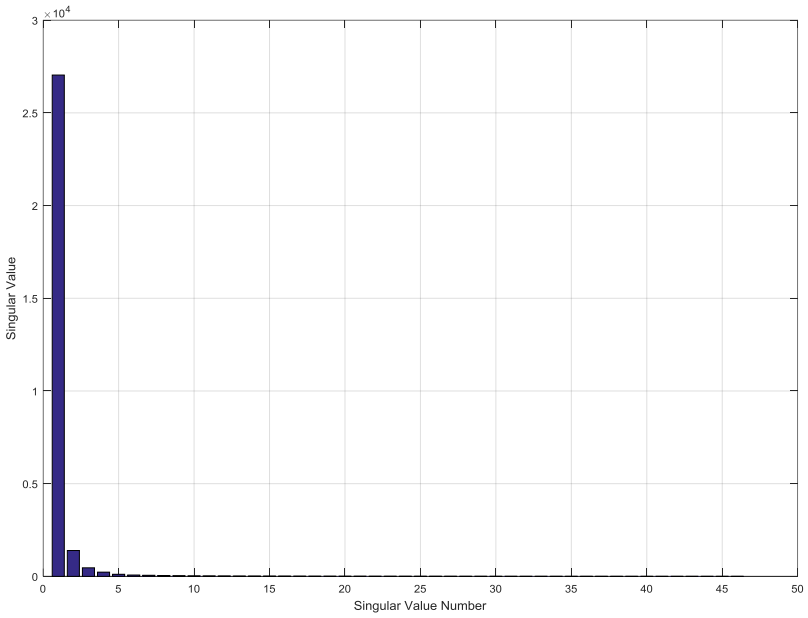

Figure 52: Singular Values from Principal Component Analysis of Temp. Measurements

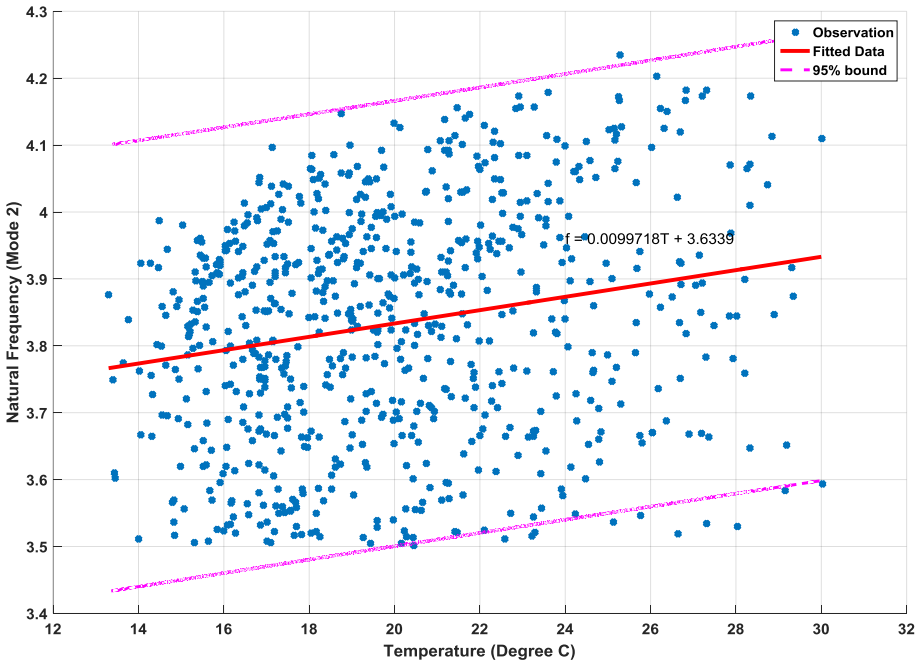

Figure 53: Relation of Natural Frequencies (2nd mode) to Temp. of the California Bridge

Table 11: Comparison of the Goodness of Fit (R2) for Linear, ARX and NARX Models

	Mode 1			Mode 2			Mode 3		
	Linear	ARX	NARX	Linear	ARX	NARX	Linear	ARX	NARX
October	0.489	0.546	0.643	0.400	0.533	0.627	0.433	0.609	0.602

	Mode 4			Mode 5			Mode 6		
	Linear	ARX	NARX	Linear	ARX	NARX	Linear	ARX	NARX
October	0.407	0.518	0.627	0.496	0.606	0.576	0.493	0.592	0.602

Salt Lake Bridge

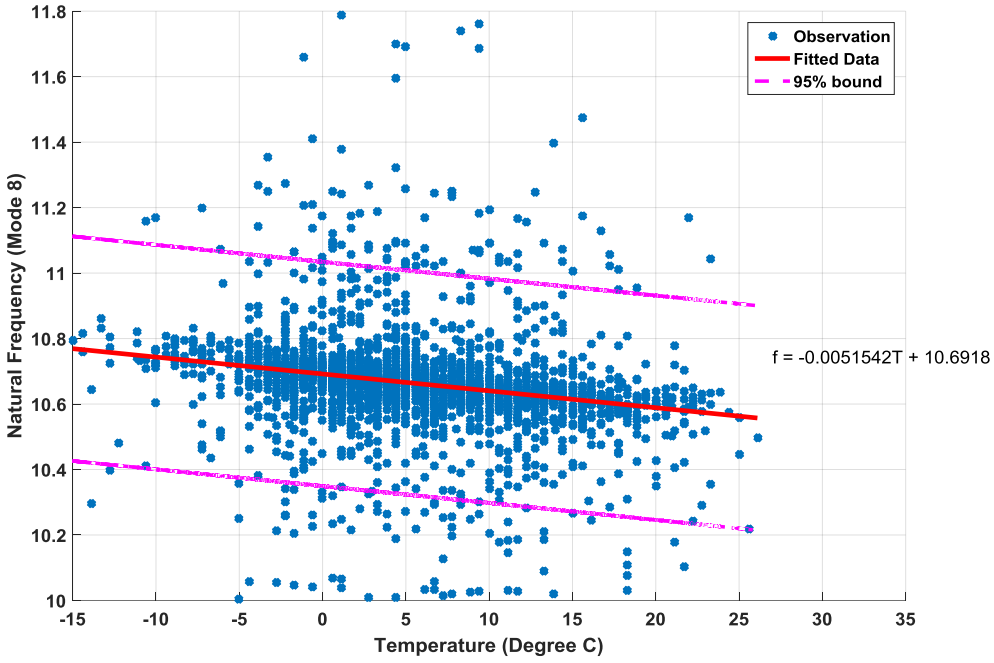

Figure 54: Relation of Natural Frequencies (8th mode) to Temp. of the Salt Lake Bridge

Table 12: Comparison of the Goodness of Fit (R2) for Linear, ARX and NARX Models

	Mode 1			Mode 2			Mode 3			Mode 4			Mode 5		
	Linear	ARX	NARX	Linear	ARX	NARX	Linear	ARX	NARX	Linear	ARX	NARX	Linear	ARX	NARX
Nov	0.141	0.451	0.455	0.200	0.464	0.495	0.148	0.419	0.506	0.161	0.349	0.384	0.103	0.504	0.445
Dec	0.132	0.512	0.421	0.191	0.438	0.391	0.164	0.398	0.402	0.176	0.432	0.517	0.198	0.466	0.426
Jan	0.156	0.421	0.436	0.150	0.480	0.458	0.123	0.392	0.475	0.115	0.489	0.478	0.174	0.395	0.489
Feb	0.161	0.498	0.564	0.152	0.483	0.393	0.175	0.452	0.470	0.124	0.391	0.386	0.145	0.447	0.459
Mar	0.165	0.569	0.546	0.167	0.420	0.401	0.199	0.380	0.374	0.192	0.519	0.482	0.187	0.495	0.498
Apr	0.138	0.426	0.328	0.182	0.405	0.504	0.167	0.422	0.418	0.159	0.477	0.379	0.187	0.395	0.484

	Mode 6			Mode 7			Mode 8			Mode 9			Mode 10		
	Linear	ARX	NARX	Linear	ARX	NARX	Linear	ARX	NARX	Linear	ARX	NARX	Linear	ARX	NARX
Nov	0.203	0.397	0.486	0.166	0.407	0.459	0.177	0.411	0.461	0.202	0.343	0.410	0.162	0.361	0.450
Dec	0.118	0.431	0.424	0.125	0.458	0.386	0.198	0.433	0.482	0.110	0.400	0.521	0.140	0.455	0.462
Jan	0.135	0.373	0.373	0.191	0.477	0.501	0.169	0.409	0.515	0.163	0.493	0.414	0.198	0.395	0.423
Feb	0.169	0.441	0.398	0.182	0.493	0.520	0.179	0.523	0.500	0.152	0.480	0.409	0.167	0.413	0.415
Mar	0.112	0.482	0.425	0.152	0.467	0.466	0.106	0.518	0.407	0.111	0.391	0.442	0.195	0.403	0.423
Apr	0.181	0.493	0.451	0.156	0.480	0.413	0.190	0.443	0.501	0.182	0.451	0.479	0.140	0.482	0.508

Chapter 6: Summary and Conclusions

A lab specimen and 3 different bridge structures with a long-term monitoring system were studied. The lab specimen was tested with impact loads every hour while temperature measurements were collected during 11 hours. The 3 bridge structures are instrumented with a long-term structural health monitoring (SHM) system that collect vibration and temperature data periodically. Findings for these structure are presented below:

Lab Specimen

This specimen was tested in an 11 hour period while the average recorded temperature was between 16.18 and 24.30 degrees Celsius. The identified frequencies change very slightly in this range of temperature. While both ends of this beam were free to expand, the support condition did not change according to the temperature increase. Since the material properties did not change significantly for this value of rise in temperature, there was not a significant change in identified frequencies consequently.

Perry Bridge

The long-term monitoring system on this bridge collected vibration measurements hourly and temperature data every 15 minutes. To investigate the effect of temperature on the dynamic characteristics of the bridge, the collected data between January 1, 2015 and June 30, 2015 (4,343 sets of data), were subjected to analysis. The Natural Excitation Technique (NExT) method along with Eigensytem Realization Algorithm (ERA) were used to extract modal parameters from ambient vibration measurements. The pattern of identified natural frequencies in this six-month period showed the variability of identified modal parameters can be as large as 19 percent while the average air temperature changed 41 degrees Celsius (-9 to 31) and the

average temperature measured on the girders of the bridge changed 27 degrees Celsius (0.32 to 27.79). Since the result of vibration-based damage detection is very dependent on the variability of the identified modal parameters, this correlation between modal parameters and temperature effects needs to be investigated in order to reduce the uncertainty for better damage identification. Three models were used to correlate temperature to natural frequencies of different modes, Linear Regression, Autoregressive model with exogenous inputs (ARX) and Nonlinear ARX model. In this study, 60 percent of the data sets were randomly selected and used for training the model, 20 percent were used as cross validation test and 20 percent were used as test sets. Even though the goodness of fit based on the calculated R^2 showed improvements by using NARX model, the associated cost with computation of potential model parameters was 15 times higher.

California Bridge

The long-term monitoring system on this bridge collected vibration measurements hourly and temperature data are collected every 15 minutes. To investigate the effect of temperature on the dynamic characteristics of the bridge, the collected data between October 1, 2015 and November 1, 2015 (720 sets of data), were subjected to analysis. The Natural Excitation Technique (NExT) method along with Eigensytem Realization Algorithm (ERA) were used to extract modal parameters from ambient vibration measurements. The pattern of identified natural frequencies in this one-month period showed the variability of identified modal parameters can be as large as 20 percent while the hourly averaged air temperature changed 26.7 degrees Celsius (13.3 to 30.0) and the hourly averaged temperature on the girders of the bridge changed 26.3 degrees Celsius (14.1 to 40.4). The identified frequencies of this bridge is increasing when temperature rises. This is contrary to the results from other bridges. Boundary conditions for this

bridge changes when temperature changes. Since the result of vibration-based damage detection is very dependent on the variability of the identified modal parameters, this correlation between modal parameters and temperature effects needs to be investigated in order to reduce the uncertainty for better damage identification. Three models were used to correlate temperature to natural frequencies of different modes, Linear Regression, Autoregressive model with exogenous inputs (ARX) and Nonlinear ARX model. In this study, 60 percent of the data sets were randomly selected and used for training the model, 20 percent were used as cross validation test and 20 percent were used as test sets. Even though the goodness of fit based on the calculated R^2 showed improvements by using NARX model, the associated cost with computation of potential model parameters was 19 times higher.

Salt Lake Bridge

The long-term monitoring system on the Salt Lake Bridge collected vibration measurements hourly. Temperature data was collected from a weather station that provided hourly temperature. To investigate the effect of temperature on the dynamic characteristics of the bridge, the collected data between November 1, 2014 and May 1, 2015 (4,338 sets of data), were subjected to analysis. The Natural Excitation Technique (NExT) method along with Eigensytem Realization Algorithm (ERA) were used to extract modal parameters from ambient vibration measurements. The pattern of identified natural frequencies in this six-month period showed the variability of identified modal parameters can be as large as 22.5 percent while the average air temperature changed 42.7 degrees Celsius (-16.7 to 26). The correlation between modal parameters and temperature effects needs to be investigated in order to reduce the uncertainty for better damage identification. Three models were used to correlate temperature to natural frequencies of different modes, Linear Regression, Autoregressive model with exogenous inputs

(ARX) and Nonlinear ARX model. In this study, 60 percent of the data sets were randomly selected and used for training the model, 20 percent were used as cross validation test and 20 percent were used as test sets. Even though the goodness of fit based on the calculated R^2 showed improvements by using NARX model, the associated cost with computation of potential model parameters was 12 times higher.

References

Alampalli, S. (1998). "Influence of in-service environment on modal parameters." *Proceedings-SPIE the International Society for Optical*, *1*, 111-116.

Brownjohn, J. M. (2007, February 15). "Structural health monitoring of civil infrastructure." *Philosophical Trans. Royal Society A: Mathmatical, Physical and Engineering Sciences, 365*(1851), 589-622.

Carder, D. S. (1937). "Observed vibrations of bridges." *Bull. Seismological Soc. Am., 27*, 267-303.

Cornwell, P., Farrar, C. R., Doebling, S., and Sohn, H. (1999, November). "Environmental variability of modal properties." *Experimental Techniques, 23*(6), 45-48.

Farrar, C. R., and Jauregui, D. A. (1998). "Comparative study of damage identification algorithms applied to a bridge: I. Experiment." *Smart Materials and Structures, 7*(5), 704.

Giraldo, D. F., Dyke, S. J., and Caicedo, J. M. (2006). "Damage detection accommodating varying environmental conditions." *Structural Health Monitoring, 5*(2), 155-172.

Google Maps. (2015). Retrieved November 2015, from Google Maps: https://www.google.com/maps

Sohn, H., Farrar, C. R., and Czarnecki, J. J. (2002). "A review of structural health monitoring literature: 1996-2001." Los Alamos Narional Laboratory, Los Alamos, New Mexico.

Xia, Y., Chen, B., Weng, S., Ni, Y.-Q., and Xu, Y.-L. (2012, May). "Temperature effect on vibration properties of civil structures: a literature review and case studies." *J. Civil Structural Health Monitoring, 2*(1), 29-46.